1521-0111/100/4/372–387$35.00
MOLECULAR PHARMACOLOGY

https://doi.org/10.1124/molpharm.121.000336
Mol Pharmacol 100:372–387, October 2021

Pharmacological Characterization of the Imipridone Anticancer Drug ONC201 Reveals a Negative Allosteric Mechanism of Action at the D_2 Dopamine Receptor[S]

R. Benjamin Free, Caroline A. Cuoco, Bing Xie, Yoon Namkung, Varun V. Prabhu, Blair K.A. Willette, Marilyn M. Day, Marta Sanchez-Soto, J. Robert Lane, Stéphane A. Laporte, Lei Shi, Joshua E. Allen, and David R. Sibley

Molecular Neuropharmacology Section, National Institute of Neurologic Disorders and Stroke, National Institutes of Health, Bethesda, Maryland (R.B.F., C.A.C., B.K.A.W., M.M.D., M.S-S., D.R.S.); Chimerix, Inc., Durham, North Carolina (V.V.P., J.E.A.); Computational Chemistry and Molecular Biophysics Section, Molecular Targets and Medications Discovery Branch, National Institute on Drug Abuse, National Institutes of Health, Baltimore, Maryland (B.X., L.S.); Department of Medicine, Research Institute of the McGill University Health Center (RI-MUHC), McGill University, Montréal, Canada (Y.N., S.A.P.); and Centre of Membrane Proteins and Receptors, Universities of Birmingham and Nottingham, Nottingham, Midlands, United Kingdom (J.R.L.)

Received June 11, 2021; accepted July 26, 2021

ABSTRACT

ONC201 is a first-in-class imipridone compound that is in clinical trials for the treatment of high-grade gliomas and other advanced cancers. Recent studies identified that ONC201 antagonizes D2-like dopamine receptors at therapeutically relevant concentrations. In the current study, characterization of ONC201 using radioligand binding and multiple functional assays revealed that it was a full antagonist of the D2 and D3 receptors (D2R and D3R) with low micromolar potencies, similar to its potency for antiproliferative effects. Curve-shift experiments using D2R-mediated β-arrestin recruitment and cAMP assays revealed that ONC201 exhibited a mixed form of antagonism. An operational model of allostery was used to analyze these data, which suggested that the predominant modulatory effect of ONC201 was on dopamine efficacy with little to no effect on dopamine affinity. To investigate how ONC201 binds to the D2R, we employed scanning mutagenesis coupled with a D2R-mediated calcium efflux assay. Eight residues were identified as being important for ONC201's functional antagonism of the D2R. Mutation of these residues followed by assessing ONC201 antagonism in multiple signaling assays highlighted specific residues involved in ONC201 binding. Together with computational modeling and simulation studies, our results suggest that ONC201 interacts with the D2R in a bitopic manner where the imipridone core of the molecule protrudes into the orthosteric binding site, but does not compete with dopamine, whereas a secondary phenyl ring engages an allosteric binding pocket that may be associated with negative modulation of receptor activity.

SIGNIFICANCE STATEMENT

ONC201 is a novel antagonist of the D2 dopamine receptor with demonstrated efficacy in the treatment of various cancers, especially high-grade glioma. This study demonstrates that ONC201 antagonizes the D2 receptor with novel bitopic and negative allosteric mechanisms of action, which may explain its high selectivity and some of its clinical anticancer properties that are distinct from other D2 receptor antagonists widely used for the treatment of schizophrenia and other neuropsychiatric disorders.

Introduction

Dopamine receptors belong to the G protein coupled receptor (GPCR) superfamily and are divided into two subfamilies, D1-like (D1R and D5R) and D2-like (D2R, D3R, and D4R) on the basis of their sequence homology, signaling properties, and pharmacology (Sibley and Monsma, 1992). D1-like receptors couple to Gs/Golf proteins to stimulate adenylyl cyclase activity and increase intracellular levels of cAMP (Beaulieu and Gainetdinov, 2011). In contrast, D2-like receptors couple to Go/Gi/

This project was funded by the Intramural Research Programs of the National Institute of Neurologic Disorders and Stroke [project ZIA-NS002263] (to D.R.S.) and the National Institute on Drug Abuse [project Z1A-DA000609] (to L.S.) at the National Institutes of Health, United States, as well as National Health and Medical Research Council (NHMRC, Australia) Project [Grant APP1049564] to J.R.L.

Varun V. Prabhu and Joshua E. Allen are employees and shareholders of Chimerix, Inc.

https://dx.doi.org/10.1124/molpharm.120.000336.

[S] This article has supplemental material available at molpharm.aspetjournals.org.

ABBREVIATIONS: BRET, bioluminescence resonance energy transfer; CAMYEL, cAMP sensor using YFP-Epac-RLuc; ClpP, caseinolytic protease P; D2R, D2 dopamine receptor; D3R, D3 dopamine receptor; D4R, D4 dopamine receptor; GPCR, G protein coupled receptor; HEK, human embryonic kidney; MD, molecular dynamics; NAM, negative allosteric modulator; ONC201, 7-benzyl-4-(2-methylbenzyl)-1,2,6,7,8,9-hexahydroimidazo [1,2-a]pyrido [3,4-e]pyrimidin- 5(1H)-one; PDB, Protein Data Bank; PEI, polyethylenimine; PTX, pertussis toxin; Rluc8, Renilla Luciferase 8; SBP, secondary binding pocket; TM, transmembrane segment; TRAIL, TNF-related apoptosis-inducing ligand.

Gz proteins to inhibit adenylyl cyclase activity and to also modulate the activities of various ion channels (Beaulieu and Gainetdinov, 2011). Recently, both D1- and D2-like receptors have also been shown to signal through β-arrestin–mediated pathways (Beaulieu and Gainetdinov, 2011; Urs et al., 2011; Harris and Urs, 2021). Together, these receptors mediate the diverse effects of dopaminergic signaling, including the regulation of mood, reward, movement, and cognition. Not surprisingly, they also serve as drug targets for the treatment of numerous pathologies, including hypertension, Parkinson disease, schizophrenia, and other neuropsychiatric disorders (Moritz et al., 2018).

Among the D2-like receptors, the D2R is an extremely well validated drug target for the therapy of both Parkinson disease (agonists) and schizophrenia (antagonists) (Moritz et al., 2018). Notably, a role for the D2R in oncology and anticancer therapy has recently begun to emerge. Several studies have shown that D2R is overexpressed in a range of malignancies (Coufal et al., 2010; Li et al., 2014; Cherubini et al., 2016; Mu et al., 2017), and that elevated D2R expression is associated with a poor clinical prognosis (Meredith et al., 2006; Mu et al., 2017; Prabhu et al., 2019). In addition to paracrine dysregulation of the dopamine pathway in tumors localized to dopamine-rich tissues, evidence for autocrine dysregulation has emerged where some tumors can also synthesize and secrete dopamine (Caragher et al., 2019; Tegowski et al., 2019). Furthermore, D2R silencing or antagonism in preclinical models has been shown to confer proapoptotic and antiproliferative antitumor effects that involve inactivation of prosurvival signaling pathways, such as mitogen-activated protein kinase and protein kinase B serine/threonine-specific protein kinase (Meredith et al., 2006; Sachlos et al., 2012; Li et al., 2014; Tegowski et al., 2019). These studies suggest that attenuation of D2R signaling may play a therapeutic role in specific forms of human cancer if targeted appropriately.

ONC201, 7-benzyl-4-(2-methylbenzyl)-1,2,6,7,8,9- hexahydroimidazo [1,2-a]pyrido [3,4-e]pyrimidin- 5(1H)-one, is a small molecule that is the founding member of the imipridone class of compounds that share a unique heterocyclic pharmacophore. This anticancer compound is in late-stage clinical development for H3 K27M-mutant gliomas after the observation of micromolar intratumoral drug concentrations in glioblastoma patients, as well as therapeutic intratumoral pharmacodynamics and durable responses to monotherapy in biomarker-defined subsets of high-grade glioma (Prabhu et al., 2020). The anticancer activity of ONC201 was originally identified in a target-agnostic, phenotypic screen for small molecule p53–independent inducers of TNF-related apoptosis-inducing ligand (TRAIL) in tumor cells (Allen et al., 2013, 2015). Tumor cell signaling studies revealed that ONC201 causes a dual inactivation of the kinases protein kinase B serine/threonine-specific protein kinase and extracellular signal-regulated kinase resulting in the dephosphorylation of the transcription factor FOXO3a. Dephosphorylated FOXO3a translocates to the nucleus resulting in upregulation of TRAIL as one of its direct target genes. ONC201 and related imipridones have also been found to activate mitochondrial caseinolytic protease P (ClpP) leading to an integrated stress response resulting in tumor cell death (Graves et al., 2019; Ishizawa et al., 2019). Recently, using a machine learning–based drug-target identification algorithm, it was predicted and confirmed that ONC201 also binds to and antagonizes the D2R (Madhukar et al., 2019), suggesting that this activity may contribute to its anticancer effects.

In the current study, we characterize the pharmacological interactions of ONC201 with all D2-like dopamine receptor subtypes and show that it is a highly selective antagonist of both the D2R and D3R. We further investigated ONC201's ability to antagonize the D2R and found that it inhibits multiple D2R-mediated signaling pathways, including Rho activation. Notably, ONC201 appeared to exhibit a mixed form of antagonism at the D2R, suggesting an allosteric component to its mechanism of action. Alanine scanning mutagenesis identified D2R residues involved in ONC201 binding, which in turn enabled computational modeling and simulation studies to characterize the D2R binding pose of ONC201. Our results suggest that ONC201 interacts with the D2R in a bitopic manner where the imipridone core of the molecule protrudes into the orthosteric site, whereas a pendant phenyl ring engages a secondary allosteric binding pocket that may confer negative allosteric modulation of receptor activity. This latter activity may play an important role in the unique and clinically validated ability of ONC201 to efficaciously antagonize D2R signaling in tumors.

Materials and Methods

Materials and Reagents. ONC201 and isomer [4,3-d] were obtained from Oncoceutics, Inc. Pertussis toxin was obtained from Sigma, and YM-254890 was purchased from FUJIFILM Wako Chemicals. Coelenterazine-H and Coelenterazine 400a were purchased from Nanolight Technology. Mutant receptor constructs were prepared by Bioinnovatise (Rockville, MD). Constructs were prepared in pcDNA3.1 vectors, and inserts were verified by sequencing. All tissue culture media and supplies were obtained from Thermo Fisher Scientific (Carlsbad, CA). All other compounds and chemicals, unless otherwise noted, were obtained from Sigma-Aldrich (St. Louis, MO).

Cell Culture and Transfection. Human embryonic kidney (HEK) 293 cells were cultured in Dulbecco's modified Eagle's medium supplemented with 10% fetal bovine serum, penicillin (100 U/ml), and streptomycin (100 μg/ml). CHO-K1-EA cells were cultured in Ham's F12 media supplemented with 10% fetal bovine serum, penicillin (100 U/ml), streptomycin (100 μg/ml), hygromycin (300 μg/ml), and G418 (800 μg/ml). Cells were grown at 37°C in 5% CO_2 and 90% humidity. HEK293 cells were seeded in 100- or 35-mm plates and transfected overnight using a 1:3 ratio [1 μg of DNA: 3 μl of polyethyleneimine (PEI)] diluted to 1 ml in nonsupplemented Dulbecco's modified Eagle's medium and added (100 μl/ml) to the cells already in culture media. Media were replaced with complete media the following day. Concentrations of DNA are indicated for each experiment type. The cells were routinely checked and found to be negative for mycoplasma infection.

cAMP Accumulation Assay. D2R- and D4R-mediated inhibition of forskolin-stimulated cAMP production was measured by using the TR-FRET–based LANCE cAMP assay (PerkinElmer, Inc., Waltham, MA). CHO-K1 cells stably expressing D2R or D4R were plated in Hanks' balanced salt solution (with $CaCl_2$ and $MgCl_2$) with 5 mM HEPES buffer and 0.2 mM sodium metabisulfite at a density of 1×10^6 cells/ml and 5 μl per well in 384-well white-bottom plates. Compounds and forskolin were made in the same buffer. Immediately after plating, cells were treated with 2.5 μl of varying concentrations of compound and 2.5 μl of forskolin (10 μM final concentration) and incubated for 30 minutes at room temperature. When running assays in antagonist mode, the EC_{80} of dopamine (10 nM) was added with the forskolin solution. Eu-cAMP tracer (5 μl) and ULight-anticAMP

(5 μl) solutions were added to each well according to the manufacturer's protocol, and cells were incubated in the dark for 2 hours at room temperature. Plates were read on a PHERAstar plate reader (BMG LABTECH, Cary, NC) with excitation at 337 nm and emission at 620 and 665 nm. Data were obtained as the ratio between A (excitation at 337 nm/emission at 665 nm) and B (excitation at 337 nm/emission at 620 nm). Values were normalized to a percentage of the control TR-FRET signal seen with a maximum concentration of dopamine for agonist mode assays or the EC_{80} concentration of dopamine for antagonist-mode assays. The Hill coefficients of the concentration-response curves did not significantly differ from unity, with the data fitting to a single site model.

DiscoverX β-arrestin Recruitment Assay. Assays were conducted with minor modifications as previously published by our laboratory (Luderman et al., 2018; Moritz et al., 2020b) using the DiscoverX PathHunter technology (DiscoverX, Inc., Fremont, CA). Briefly, CHO-K1-EA cells stably expressing β-arrestin fused to an N-terminal deletion mutant of β-galactosidase and human D2R, D3R, or D4R fused to a complementing N-terminal fragment of β-galactosidase (DiscoverX, Inc.) were maintained in Ham's F12 media supplemented with 10% fetal bovine serum, 100 U/ml penicillin, 100 ug/ml streptomycin, 800 μg/ml G418, and 300 ug/ml hygromycin at 37°C, 5% CO_2, and 90% humidity. Cells stably expressing D2R, D3R, or D4R were seeded at a density of 2625 cells/well and 7.5 μl/well in 384-well black-bottomed plates. After 16–24 hours of incubation, cells were treated with multiple concentrations of compound in PBS containing 0.2 mM sodium metabisulfite and incubated at 37°C for 90 minutes. DiscoverX reagent was added to cells according to the manufacturer's recommendations and incubated for 45 minutes at room temperature. Luminescence was measured on a Hamamatsu FDSS μCell reader. Data were collected as relative luminescence units and subsequently normalized to control compound as indicated for each figure. The Hill coefficients of the concentration-response curves did not differ from unity with the data fitting to a single site model.

Radioligand Binding Assay. Radioligand competition binding assays were conducted with slight modifications as previously described by our laboratory (Luderman et al., 2018; Moritz et al., 2020b; Sanchez-Soto et al., 2020). CHO-K1 cells stably expressing human D2R or D3R were dissociated from plates using Earle's balanced salt solution lacking calcium and magnesium, and intact cells were collected by centrifugation at 1000*g* for 10 minutes. Cells were resuspended and lysed using hypotonic lysis buffer (5 mM Tris-HCl and 5 mM $MgCl_2$ at pH 7.4) at 4°C. Cell lysate was pelleted by centrifugation at 30,000*g* for 30 minutes and resuspended in Earle's balanced salt solution + $CaCl_2$ at pH 7.4. Cell lysates (100 μl, containing ~10 to 20 μg of protein, quantified by the Bradford assay) were incubated for 90 minutes at room temperature with 0.2 to 0.3 nM [^{3}H]methylspiperone and the indicated concentrations of ONC201 in a final reaction volume of 250 μl. Nonspecific binding was determined in the presence of 4 μM (+)-butaclamol. Bound radioligand was separated from free by filtration through a PerkinElmer UniFilter-96 Harvester (PerkinElmer, Waltham, MA), washing three times with ice-cold assay buffer (1 ml per well). After drying, 50 μl of liquid scintillation cocktail (MicroScint PS; PerkinElmer) was added to each well, and plates were sealed and quantified using a PerkinElmer Topcount NXT.

G_{12} and Rho BRET Assays. BRET assays for detecting G_{12} or Rho activation were performed as previously described (Namkung et al., 2018). Briefly, HEK293 cells were seeded at a density of 1×10^6 cells per 100-mm dish and transfected the next day with 3 μg of D2R cDNA with 240 ng $G\alpha_{12}$(136)-RlucII, 600 ng GFP10-$G\gamma_1$, and 600 ng FLAG-$G\beta$1 for measuring G_{12} BRET activation. To measure Rho activation, the cells were transfected with 1 μg of D2R cDNA with 120 ng protein kinase N1-Rhobinding domain-RlucII and 900 ng rGFP-CAAX using PEI methods as described previously (Boussif et al., 1995). Briefly, a total 6 μg of DNA in 0.5 ml of PBS was mixed with 12 μl of PEI (1 mg/ml) in 0.5 ml PBS and then incubated for 20 minutes at RT prior to applying to the cells. After 24 hours, cells were detached and seeded onto polyornithine-coated 96-well white plates at a density of 25,000 cells per well for the BRET assays, which were performed 48 hours after transfection.

On the day of the BRET assays, the cells were washed once with Tyrode's buffer (140 mM NaCl, 2.7 mM KCl, 1 mM $CaCl_2$, 12 mM $NaHCO_3$, 5.6 mM D-glucose, 0.5 mM $MgCl_2$, 0.37 mM NaH_2PO_4, 25 mM HEPES, pH 7.4) and left in Tyrode's buffer at 37°C in a CO_2 incubator until use. For the G_{12} BRET assay, the cells were stimulated with various concentrations of dopamine plus 0.2 mM sodium metabisulfite and/or ONC201 for 10 minutes at 37°C before BRET assessment. For the Rho BRET assay, the cells were treated with either vehicle (Tyrode's buffer or 0.02% DMSO), 100 ng/ml of pertussis toxin (PTX) (overnight), or 200 nM of YM-254890 for 30 minutes at 37°C and then stimulated with various concentrations of dopamine for 2.5 minutes at RT before BRET assessment. For antagonist-mode assays, the cells were stimulated with either 1 μM or 10 μM of dopamine in the presence of various concentrations of sulpiride or ONC201. BRET signals were measured 3–5 minutes after addition of coelenterazine 400a to a final concentration of 5 μM using a Synergy2 (BioTek) microplate reader. Filter set was 410/80 nm and 515/30 nm for detecting the RlucII *Renilla* luciferase (donor) and GFP10/rGFP (acceptor) light emission, respectively. The BRET ratio was determined by calculating the ratio of the light emitted by GFP10/rGFP over the light emitted by the RlucII.

G_o BRET Assay. HEK293 cells were seeded at a density of 4×10^6 cells per 100-mm dish and incubated overnight. The next day, cells were transfected with 0.5 μg $G_{\alpha o1}$-RLuc8, along with 5 μg $G_{\gamma 2}$-mVenus, 4 μg $G_{\beta 1}$, and 5 μg of the corresponding untagged receptor vectors using PEI (DNA:PEI, 1:3 ratio). At 48 hours after transfection, cells were harvested, washed, and resuspended in Dulbecco's phosphate-buffered saline containing 0.2 mM sodium metabisulfite and 5.5 mM glucose. Cells were then plated in 96-well, white, solid-bottomed plates (Greiner Bio-One) and incubated in the dark for 45 minutes. Dose-response curves were performed by adding 5 μM coelenterazine-h (NanoLight Technology) for 5 minutes, followed by addition of the indicated concentrations of compounds for 5 minutes. BRET signals were determined by calculating the ratio of the light emitted by mVenus (535/30 nm) over that emitted by Rluc8 (475/30 nm) using a PHERAstar plate reader (BMG LABTECH, Cary, NC). Net BRET values were obtained by subtracting the background ratio from vehicle-treated wells. Agonist-promoted BRET changes were expressed as a percentage of the maximum response of the wild-type receptor for each ligand.

CAMYEL cAMP BRET Assay. Measurement of cAMP accumulation using the CAMYEL BRET biosensor was performed as described previously (Jiang et al., 2007; Sanchez-Soto et al., 2020). Briefly, HEK293 cells were seeded at a density of 4×10^6 cells per 100-mm dish. The next day, cells were transfected with 5 μg of untagged receptor vector and 5 μg of CAMYEL biosensor (Jiang et al., 2007) using PEI (1:3 ratio, DNA:PEI). At 48 hours after transfection, cells were harvested, washed, and resuspended in Dulbecco's phosphate-buffered saline containing 0.2 mM sodium metabisulfite and 5.5 mM glucose. Cells were then plated in 96-well, white, solid-bottomed plates (Greiner Bio-One) and incubated in the dark for 45 minutes. To measure inhibition of cAMP accumulation, cells were pretreated for 5 minutes with 10 μM forskolin and 10 μM propranolol (to block endogenous β-adrenergic receptors) followed by the addition of 5 μM coelenterazine-h. Cells were then incubated for 5 minutes with indicated compounds, and the BRET signal was determined by calculating the ratio of the light emitted by mVenus (535/30 nm) over that emitted by Rluc8 (475/30 nm) using a PHERAstar plate reader (BMG LABTECH, Cary, NC). The net BRET values were obtained by subtracting the background ratio from vehicle-treated cells. Agonist-promoted BRET changes were expressed as a percentage of the maximum response of the wild-type receptor for each ligand.

GPCR Profiling. To determine the GPCR selectivity profiles of ONC201 and haloperidol, these compounds were screened using the DiscoverX gpcrMAX GPCR panel, which measures the GPCR activation of β-arrestin recruitment to different GPCRs (see DiscoverX β-arrestin recruitment assay methods above). This study was conducted by DiscoverX, Inc. (Fremont, CA). β-arrestin recruitment to each GPCR in the panel was stimulated by an agonist for that specific GPCR in the presence of either 10 μM ONC201 or 10 μM haloperidol. Assay results, run in duplicate, are presented as the mean percent inhibition of the indicated GPCR for each compound tested. Only responses that deviate >20% from baseline are considered significant. For a full description of the DiscoverX gpcrMAX GPCR panel, see http://www.DiscoverX.com.

Alanine Scanning Mutagenesis and Ca^{2+} Mobilization Assay. The D2R alanine scan mutant library was created by mutating residues 2–443 of the human D2R long isoform (444 total residues in length) to alanines (with wild-type alanines changed to serines). Each of the resulting 442 clones was verified by DNA sequencing. Functional activity of each clone was assessed using a Ca^{2+} mobilization assay as previously described (Greene et al., 2011). Briefly, HEK293T cells were transiently transfected with each D2R clone along with a chimeric $G_{\alpha 16}$ subunit containing 44 residues of rat gustducin and then plated in poly-D-lysine coated, black 384-well plates with clear bottoms and incubated for 22 hours at 37°C. Growth media was removed, and the cells were washed twice with Hanks' balanced salt solution containing 20 mM HEPES then loaded with a Ca^{2+} indicator dye in Hanks' balanced salt solution containing 20 mM HEPES (calcium 4 assay kit, Molecular Devices). Cells were incubated at 37°C for 1 hour in the presence of dye, then moved to a Flexstation II-384 (Molecular Devices) set for 32°C. After a 15-minute temperature equilibration (without washout), indicated compounds were injected (at t = 20 seconds), and fluorescence was measured for 100 to 180 seconds, reading every 3 seconds. Data sets were analyzed and represented as % over baseline signal using Prism 5.0 software (GraphPad Software, Inc).

Molecular Docking. The molecular modeling and docking procedures described below were carried out with the Schrodinger Suite (version 2020-4). Specifically, the compound structures were prepared and parameterized with the LigPrep and Epik modules. The missing torsion parameters were acquired by the Forcefield Builder. The D2R structures in inactive (Im et al., 2020) (PDB: 7DFP) and active (Yin et al., 2020) (PDB: 6VMS) states were prepared with the Protein Preparation Wizard. The induced-fit docking was performed with the extended sampling protocol. Hierarchy clustering in the conformer cluster module was used to select representative docking poses.

Molecular Dynamics Simulations. In the D2R active state structure (PDB: 6VMS), the N terminus and the N-terminal region of TM1 are missing and distorted as well. To prevent the lipid molecules from entering into the binding pocket from this incomplete portion of transmembrane domain during MD simulations, we built part of the N terminus starting from residue Q16 and the complete TM1 with Modeler (version 9.24) (Sali and Blundell, 1993). Using the resulting D2R model, we docked and selected representative poses of ONC201 with dopamine bound in the orthosteric site. The resulting complex models were then embedded in a 1-palmitoyl-2-oleoylphosphatidylcholine lipid bilayer with explicit water using Desmond System Builder in Schrodinger Suite (version 2020-4). The Na^+ and Cl^- ions were added to neutralize the system and to make the salt concentration of the system to be 150 mM. MD simulations were carried out using Desmond MD System (version 6.1; D.E. Shaw Research, New York, NY) (Bowers et al., 2006) with the OPLS3e force field (Roos et al., 2019). For both the equilibrations and the following unrestrained production runs, we used Langevin constant pressure and temperature dynamical system to maintain 1 atm pressure and 310K temperature on an anisotropic flexible periodic cell. After the simulation systems were minimized and equilibrated with restraints on the heavy atoms of the ligands and protein backbone for 18 ns, a 1200 ns MD trajectory was collected for each of two poses described in *Results*.

Analysis of Functional Data. GraphPad Prism 9.1.2 (San Diego, CA) was used for all statistical analysis, nonlinear regression, and simulations. All concentration-response curve data were analyzed using the modified four-parameter Hill equation to derive potency estimates (https://www.graphpad.com/):

$$E = \text{basel} + \frac{(E_{\max} - \text{basel}) \cdot [A]^{nH}}{[A]^{nH} + EC_{50}^{nH}},$$

Where E is the effect of the system, n_H is the Hill slope, and EC_{50} is the concentration of agonist [A] that gives the midpoint response between basal and maximal effect (E_{max}) of dopamine or other agonists, which are the lower and upper asymptotes of the response, respectively.

Functional data describing the interaction between ONC201 and dopamine at the D2R were analyzed using a complete operational model of allosterism and agonism (Leach et al., 2007) according to the following equation:

$$E = E_m \frac{(\tau_A[A](K_B + \alpha\beta[B]) + \tau_B[B]K_A)^{nH}}{([A]K_B + K_AK_B + K_A[B] + \alpha[A][B])^{nH} + (\tau_A[A](K_B + \alpha\beta[B]) + \tau_B[B]K_A)^{nH}},$$

Where E_m is the maximum possible cellular response, [A] and [B] are the concentrations of orthosteric (dopamine) and allosteric (ONC201) ligands, respectively, K_A and K_B are the equilibrium dissociation constant of the orthosteric and allosteric ligands, respectively, τ_A and τ_B (constrained to 0.001 to reflect no detectable efficacy) are operational measures of orthosteric and allosteric ligand efficacy, respectively, that incorporate both signal efficiency and receptor density, n_H is the Hill slope of the orthosteric agonist concentration-response curve, α is the binding cooperativity parameter between the orthosteric and allosteric ligand, and β denotes the magnitude of the allosteric effect of the modulator on the efficacy of the orthosteric agonist. Increasing concentrations of ONC201 caused a decrease in E_{max} that did not reach a limit within the concentration range used. To fit the model to these data, β was constrained to 0.001 to denote high negative cooperativity with dopamine efficacy. Values of α and/or β greater than 1 denote allosteric potentiation, whereas values less than 1 (but greater than 0) denote allosteric inhibition. Our fits derived estimates of α that were close to 0. We used an extra sum of squares F-test to compare the fit of these data when α was constrained to 0 or was not constrained and found that the simpler model (when $\alpha = 0$) was preferred ($P > 0.05$).

Statistical Analyses. Unless otherwise indicated, data were analyzed using GraphPad Prism 8.4.0 (GraphPad Software, Inc., La Jolla, CA). All results are normalized to dopamine control. Maximum efficacies are expressed as mean ± S.D. Affinities and potencies are expressed as geometric mean [95% confidence interval]. Statistical significance was determined using two-tailed Student's t tests when two groups were compared and one-way ANOVA with Bonferroni test when multiple groups were compared, with $P < 0.05$ used as the cutoff for statistical significance.

Results

ONC201 is a Selective D2R/D3R Antagonist. Since prior studies (Madhukar et al., 2019; Prabhu et al., 2019) suggested that the D2R is a potential target that is directly involved in the antiproliferative and anticancer effects of ONC201 (Fig. 1A), we sought to characterize its interaction mechanism with the D2R. As many compounds that interact with the D2R also exhibit cross reactivity at other GPCRs, ONC201 was screened for functional activity in a panel of

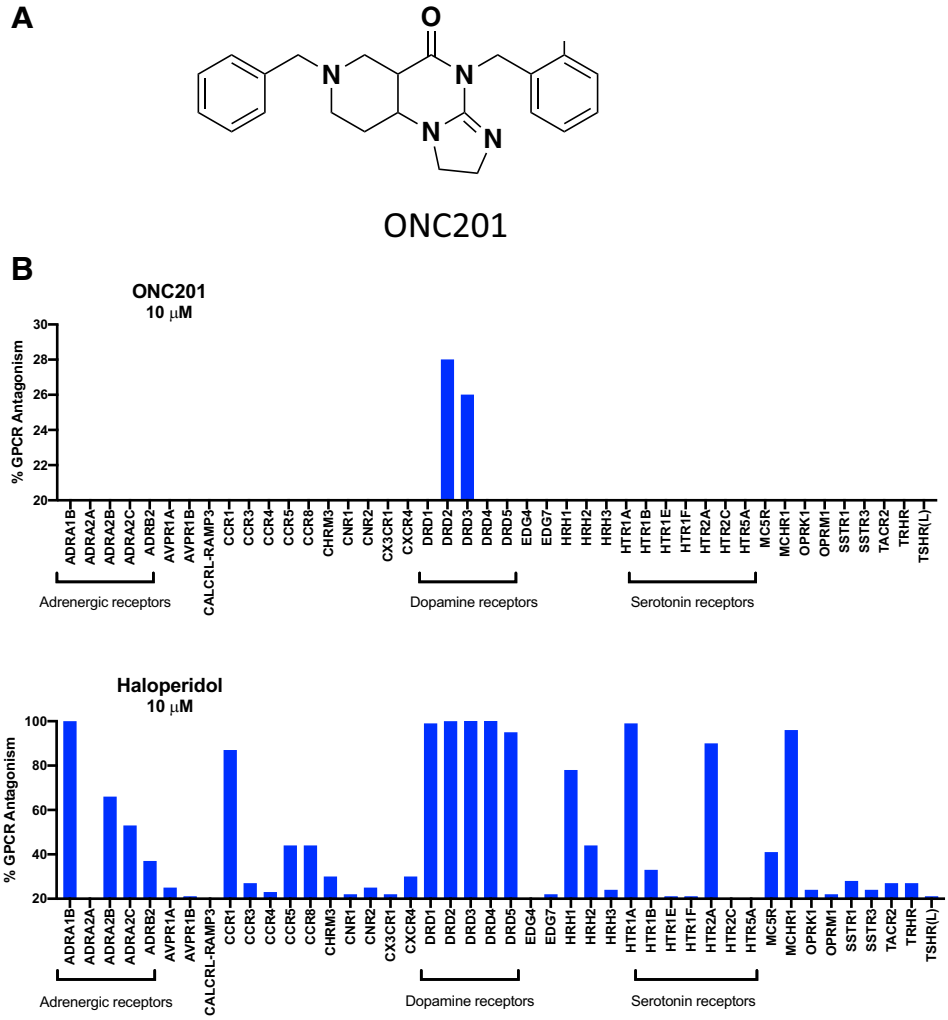

Fig. 1. ONC201 shows high D_2-like receptor selectivity. (A) Structure of the imipridone ONC201. (B) Screening panels demonstrating antagonism by ONC201 (top) or haloperidol (bottom) of agonist-stimulated β-arrestin recruitment to various GPCRs. The GPCR screening study was performed by DiscoverX, Inc. (Fremont, CA). Briefly, cells were preincubated with 10 μM of either ONC201 or haloperidol followed by an EC_{80} concentration of agonist for each indicated receptor (dopamine was the agonist used for dopamine receptors). β-arrestin recruitment was detected through the addition of DiscoverX PathHunter detection reagent cocktail. Microplates were read with a PerkinElmer EnvisionTM instrument for chemiluminescent signal detection. Assay results, run in duplicate, are presented as the mean percent inhibition of the indicated GPCR for each compound tested. Compound activity was analyzed using the CBIS data analysis suite (ChemInnovation, CA) and expressed as a percentage of the antagonism observed, as adapted from (Prabhu et al., 2018). Note that in (A), the *y*-axis does not extend to 100%. For a full description of the DiscoverX gpcrMAX assay panel see: http://www.DiscoverX.com.

diverse human GPCR targets using β-arrestin recruitment as the functional readout. As shown in the top panel of Fig. 1B, when screened in antagonist mode at a relatively high concentration (10 μM), which is achieved therapeutically in plasma and several tissues (Prabhu et al., 2020), ONC201 only blocked signaling through the D2R and D3R while lacking activity at a wide range of biogenic amine and other GPCRs (see Supplemental Table 1 for list of GPCRs). In contrast, the prototypical D2R antagonist and typical antipsychotic haloperidol exhibited its expected activity at the D2-like receptors (for which it has low nanomolar affinity), but also exhibited complete blockade of the D1-like receptors and a number of other adrenergic and serotonergic receptors for which it has affinity in the 10 nM range (Fig. 1C, bottom panel). When tested in agonist mode, neither ONC201 nor haloperidol stimulated β-arrestin recruitment to any of the tested GPCRs (data not shown). Thus, ONC201 exhibits global selectivity among GPCRs and functions primarily as a D2R/D3R antagonist.

We were next interested in quantifying the binding affinity of ONC201 at the D2R and D3R and performed radioligand binding competition assays using [^{3}H]methylspiperone, a competitive antagonist that binds to the orthosteric sites of the D2R and D3R. Figure 2 shows that ONC201 is able to completely inhibit [^{3}H]methylspiperone binding to both the D2R and D3R in a dose-dependent fashion. Using this assay, ONC201 actually exhibited slightly higher (~2-fold) binding affinity for the D3R (Ki = 30 μM) than for the D2R (Ki = 67 μM). Notably, however, the receptor binding affinities of ONC201 appeared low compared with the level of functional antagonism seen with 10 μM ONC201 in the GPCR screening panel (Fig. 1B), so we sought to further characterize ONC201-D2R/D3R interactions using functional assays.

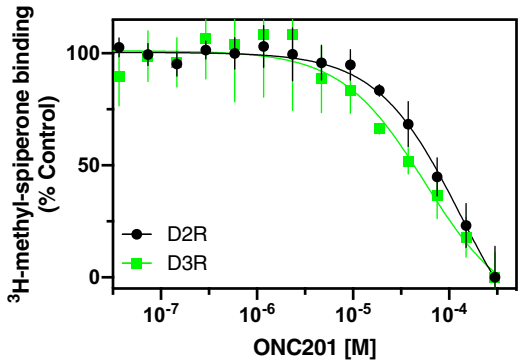

Fig. 2. Radioligand binding competition assays to determine ONC201 affinity for the D2R and D3R. Radioligand binding assays using [^{3}H]methylspiperone were performed as described in the *Materials and Methods*. Briefly, membranes from CHO cells stably expressing either the D2R or D3R were harvested and incubated with the indicated concentrations of ONC201 and 0.5 nM [^{3}H]methylspiperone. The data are expressed as percentage of the control specific binding and represent mean ± S.D. values from three independent experiments performed in triplicate. Mean ONC201 Ki values [95% C.I.] for each receptor were calculated from the IC_{50} values using the Cheng-Prusoff equation (Cheng and Prusoff, 1973) and found to be 65.6 μM [44–102] for the D2R and 27.9 μM [9.2–99] for the D3R.

We initially examined ONC201's functional interactions with the D2R using β-arrestin recruitment, the same functional assay that was used in Fig. 1. The experiment in Fig. 3A shows that ONC201 has no efficacy as an agonist in this assay but antagonized dopamine-stimulated β-arrestin recruitment with an IC_{50} of 11 μM (Fig. 3B). The competitive antagonist sulpiride was included as a positive control and exhibited an IC_{50} of 48 nM (Fig. 3B). Similarly, ONC201 lacked agonist activity for stimulating β-arrestin recruitment to the D3R (Fig. 3C) but dose-dependently inhibited dopamine-stimulated activity with an IC_{50} of 21 μM, whereas a positive control antagonist, spiperone, inhibited β-arrestin recruitment to the D3R with an IC_{50} of 5.3 nM (Fig. 3D). Thus, based on the IC_{50} values derived from the functional β-arrestin recruitment assay, ONC201 appears to be ∼6-fold and ∼2-fold more potent at the D2R and D3R, respectively, when compared with its affinities observed in the radioligand binding competition assay. Also, in contrast to the radioligand binding assay, ONC201 is ∼2-fold more potent at the D2R versus the D3R using the β-arrestin recruitment assay. We also examined ONC201's ability to antagonize agonist-simulated β-arrestin recruitment to the D4R. ONC201 lacked agonist efficacy in this assay (Fig. 3E) and only inhibited the dopamine-stimulated response at the highest concentration (100 μM) used (Fig. 3F). Taken together, these data are congruent with those observed in the functional GPCR scan shown in Fig. 1B. Further, these results indicate that ONC201 is a selective D2R/D3R versus D4R antagonist.

We next evaluated a structurally related imipridone compound that is a linear [4,3-d] isomer of ONC201 [also referred to as the [3,4-e] isomer, (Wagner et al., 2014)] (Fig. 4A). Notably, the [4,3-d] isomer does not induce cell death or affect the proliferation of cancer cells in a therapeutically relevant dose range (Wagner et al., 2014). When tested for its ability to antagonize dopamine stimulation of β-arrestin recruitment to the D2R, we found that this compound was inactive up to the highest concentration examined (100 μM) (Fig. 4B). In contrast, sulpiride effectively antagonized the dopamine response with an IC_{50} of 48 nM. When the assay was performed in a different format using dopamine concentration-response curves and increasing concentrations of the ONC201 isomer [4,3-d], similar results were observed (Fig. 4C). The potency of dopamine was not significantly affected by any concentration of the ONC201 isomer [4,3-d]. These results are consistent with the idea that antagonism of the D2R contributes to the anticancer activity of ONC201.

Next, the effects of ONC201 were evaluated on cAMP accumulation as a readout of the canonical G protein–signaling pathway for the D2R. Figure 5A shows that dopamine inhibited forskolin-stimulated cAMP accumulation with an EC_{50} of 2.3 nM. ONC201 exhibited no agonist activity in this assay but inhibited the dopamine response with an IC_{50} of 9.3 μM. This IC_{50} value is similar to that observed for ONC201 in the D2R β-arrestin recruitment assay (11 μM, Fig. 3B). Sulpiride was also observed to potently inhibit the dopamine response with an IC_{50} of 1.5 nM (Fig. 5A). Since the D3R is not robustly coupled to regulating cAMP levels, we were not able to test ONC201 in this signaling paradigm, but we were able to evaluate it using a D4R-mediated cAMP assay (Fig. 5B). As with the D2R, ONC201 was without effect as an agonist but, unlike the D2R results, it displayed minimal activity as an antagonist in the D4 cAMP assay (Fig. 5B). As the inhibition by ONC201 was less than 50% at the highest concentration tested (100 μM), we were unable to calculate an IC_{50} value. These results mirror those observed for the D4R-mediated β-arrestin recruitment assay (Fig. 3F). Taken together, these results further confirm that ONC201 is a selective D2R/D3R antagonist with similar inhibitory potencies between its effects on β-arrestin recruitment and cAMP accumulation.

ONC201 Antagonizes D2R-Mediated Rho and G_{12} Signaling. In addition to antagonizing the cAMP and β-arrestin–mediated signaling pathways, we wondered if ONC201 might play a role in regulating noncanonical D2R signaling potentially related to cancer. We noted that the small molecular weight GTPase Rho may play a role in several cancers, including glioblastoma (Fortin Ensign et al., 2013; Yu and Brown, 2015; Yu et al., 2018). Rho can be activated by different Rho guanine nucleotide exchange factors, which in turn are activated by $G_{12/13}$ proteins through various GPCRs. Given the recent availability of Rho and G_{12} BRET biosensors (Namkung et al., 2018), we wanted to use these to determine if the D2R could activate this signaling pathway. Figure 6A shows that dopamine can, in fact, potently stimulate Rho activation in D2R-transfected HEK cells with an EC_{50} of 185 nM. Rho activation was not observed in cells lacking D2R transfection (data not shown). To investigate the underlying mechanism of Rho activation, we treated the cells overnight with PTX to inactivate G_i and G_o proteins (Namkung et al., 2018), which are normally linked to the D2R. As can be seen in Fig. 6A, PTX treatment did not have an effect on dopamine-stimulated Rho activation. We next cotreated the cells with YM-254890, which is a small molecule inhibitor of $G_{q/11}$ proteins, however, this too was without effect on dopamine-stimulated Rho activation (Fig. 6A) suggesting that other G proteins, such as $G_{12/13}$, are involved. Figure 6B shows that Rho activation by dopamine can be blocked by the D2R-selective antagonist sulpiride with an IC_{50} of 63 nM. Notably, ONC201 was also able to antagonize this response with an IC_{50} of 9.4 μM, similar to its potency in blocking other D2R-mediated signaling

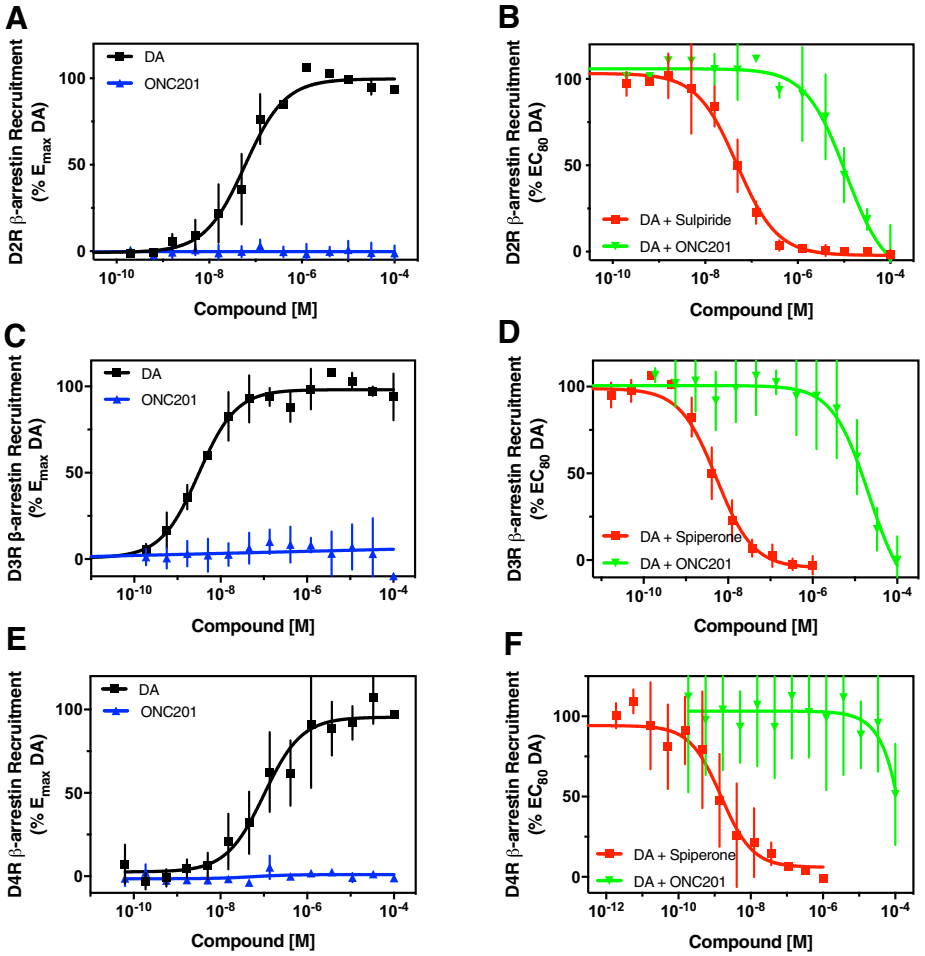

Fig. 3 Pharmacological activity of ONC201 on D_2-like dopamine receptors. β-arrestin recruitment assays were performed as described in the *Materials and Methods*. Data are expressed as a percentage of the maximum dopamine response in each assay and represent the mean ± S.D. values from 3 experiments each performed in triplicate. EC_{50} or IC_{50} values are expressed as means (95% CI). ONC201 did not produce any measurable agonist response for any of the tested receptors. (A) Dopamine stimulated β-arrestin recruitment to the D2R with an EC_{50} of 58 nM [40–86]. (B) β-arrestin recruitment to the D2R was stimulated with an EC_{80} concentration of dopamine (1 μM) and coincubated with the indicated concentrations of either sulpiride or ONC201 resulting in IC_{50} values of 48 nM [35–68] and 11 μM [5.6–21], respectively. (C) Dopamine stimulated β-arrestin recruitment to the D3R with an EC_{50} of 3 nM [2–4.7]. (D) β-arrestin recruitment to the D3R was stimulated with an EC_{80} concentration of dopamine (30 nM) and coincubated with the indicated concentrations of either spiperone or ONC201 resulting in IC_{50} values of 5.3 nM [3.8–7.5] and 21 μM [9.6–51], respectively. (E) Dopamine stimulated β-arrestin recruitment to the D4R with an EC_{50} of 100 nM [47–218]. (F) β-arrestin recruitment to the D4R was stimulated with an EC_{80} concentration of dopamine (1 μM) and coincubated with the indicated concentrations of either spiperone or ONC201 resulting in an IC_{50} value of 1.6 nM [0.6–4.5] for spiperone, whereas incomplete inhibition was observed for ONC201 ($IC_{50} > 100$ μM).

pathways (*vide supra*). As G_{12} protein–mediated signaling can lead to Rho activation, we next examined the ability of the D2R to activate G_{12} using a BRET-based assay (Namkung et al., 2018). Figure 6C shows that dopamine dose-dependently stimulates G_{12} activation with an EC_{50} of 310 nM, whereas ONC201 treatment alone had no stimulatory effect. In contrast, Fig. 6D shows that ONC201 can dose-dependently inhibit dopamine-stimulated G_{12} activation with an IC_{50} of 33 μM. Sulpiride also antagonized this response with an IC_{50} of 18 nM. To our knowledge, these data are the first to show that the D2R can couple to G_{12} and mediate Rho activation and further show that ONC201 can antagonize this signaling pathway.

ONC201 Antagonizes D2R in an Allosteric Fashion. We extended our pharmacological characterization of ONC201 by examining its mechanism of D2R antagonism. To accomplish this, we performed curve-shift experiments in which the ability of increasing concentrations of ONC201 to modulate dopamine potency and efficacy was measured. Figure 7A shows concentration-response curves for dopamine stimulation of β-arrestin recruitment in the presence of increasing concentrations of ONC201. As can be appreciated, as the concentration of ONC201 increases, there is a decrease in both the apparent potency (EC_{50}) of dopamine as well as the maximum response (E_{max}), suggesting that ONC201 exhibits a mixed form of antagonism. Analysis of these data using the operational model of allostery (Leach et al., 2007) was consistent with a highly negative modulatory effect on dopamine efficacy, such that it was necessary to constrain this parameter (β) to 0.001 to achieve a good fit to the data (see *Materials and Methods*). This fit allowed estimation of ONC201's affinity (K_b = 3 μM) and indicated no cooperativity with dopamine affinity (α = 0.2, but not significantly different from α = 0, extra sum of squares F-test, $P > 0.05$) (Table 1). Similar

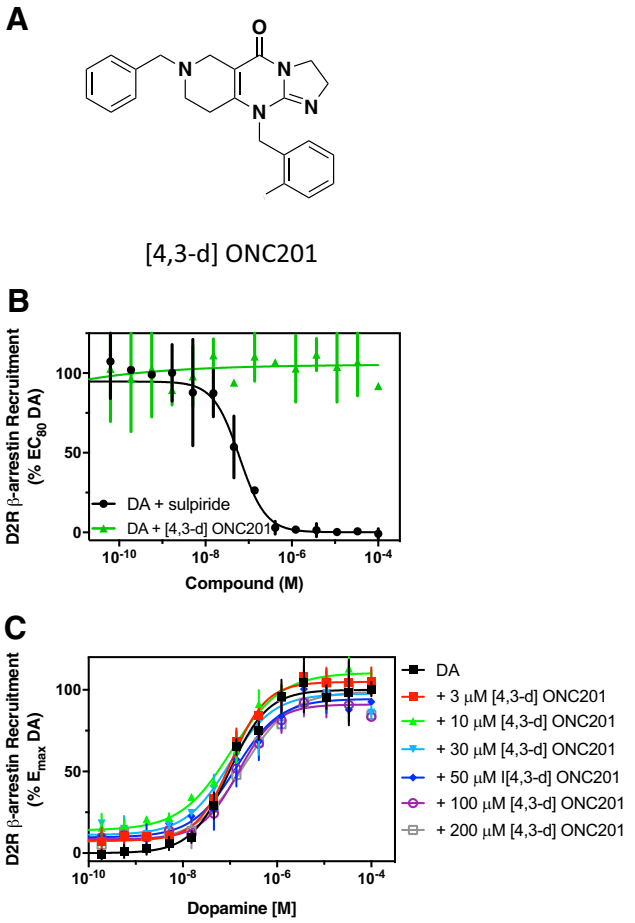

Fig. 4. ONC201 isomer [4,3-d] is inactive at the D2R. (A) Structure of ONC201 isomer [4,3-d]. (B) β-arrestin recruitment assays were performed as described in the *Materials and Methods*. Data are expressed as a percentage of the maximum dopamine response and represent the mean ± S.D. values from 3 experiments, each performed in triplicate. Cells were incubated with an EC_{80} concentration of dopamine (1 μM) in the presence of increasing concentrations of sulpiride or the ONC201 isomer [4,3-d]. Sulpiride antagonized the D2R-mediated dopamine response with an IC_{50} of 48 nM [35–68] [mean (95% CI)], while the ONC201 isomer [4,3-d] was unable to block the response. (C) Dopamine-mediated β-arrestin recruitment assays were conducted by stimulating the D2R with the indicated concentrations of dopamine with or without various concentrations of the ONC201 isomer [4,3-d]. The EC_{50} of dopamine was not significantly affected by any concentration of the ONC201 isomer [4,3-d].

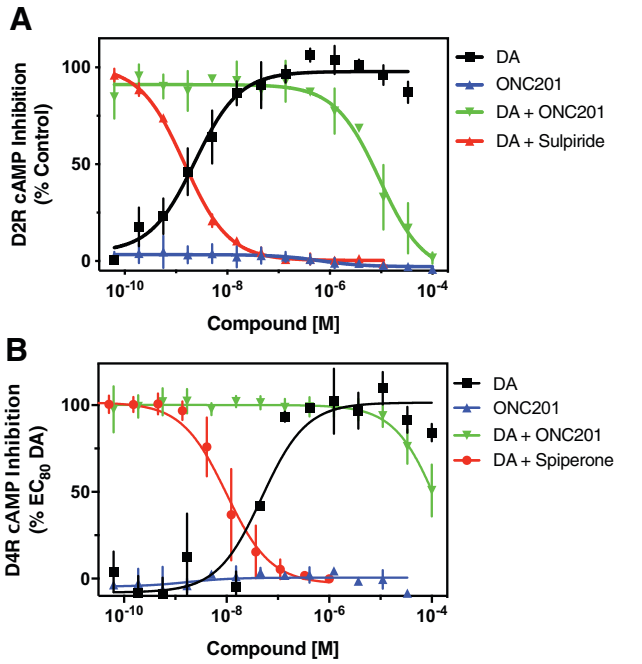

Fig. 5. Functional antagonism of D2R- and D4R-mediated inhibition of forskolin-stimulated cAMP accumulation. CHO cells stably expressing either the D2R (A) or D4R (B) were incubated with 10 μM of forskolin plus the indicated drug combinations, and the resulting cAMP levels were determined using the LANCE assay as described in the *Materials and Methods*. Data are expressed as a percentage of the inhibition observed with dopamine alone (% control) and are expressed as the mean ± S.D. values from at least 3 experiments each performed in triplicate. EC_{50} or IC_{50} values are expressed as means (95% CI). (A) ONC201 failed to show any measurable agonist response. Dopamine dose-dependently inhibited cAMP accumulation with an EC_{50} value of 2.3 nM [1.5–3.6]. For antagonist-mode assays, inhibition of cAMP accumulation by the D2R was promoted with an EC_{80} concentration of dopamine (10 nM) and coincubated with the indicated concentrations of either sulpiride or ONC201 resulting in IC_{50} values of 1.5 nM [1.3–1.7] and 9.3 μM [5.7–15], respectively. (B) ONC201 failed to show any measurable agonist response. Dopamine dose-dependently inhibited cAMP accumulation with an EC_{50} value of 0.6 nM [0.3–1.2]. For antagonist-mode assays, inhibition of cAMP accumulation by the D4R was promoted with an EC_{80} concentration of dopamine (10 nM) and coincubated with the indicated concentrations of either spiperone or ONC201, resulting in an IC_{50} value of 9.8 nM [7.9–12] for spiperone, whereas incomplete inhibition was observed for ONC201 (IC_{50} > 100 μM).

results were obtained when we examined dopamine-stimulated inhibition of cAMP accumulation (Fig. 7B) with the resulting data analysis yielding the following parameters: ONC201 K_b = 2.3 μM, β constrained to 0.001, α = 0.5 (but not significantly different from α = 0, extra sum of squares F-test, $P > 0.05$) (Table 1). Taken together, these data suggest that ONC201 displays limited cooperativity with dopamine affinity but exhibits a highly negative modulatory effect on dopamine efficacy, which is consistent with an allosteric mechanism of action. These curve-shift data contrast with those observed for sulpiride, a purely competitive antagonist of the D2R, which only affects dopamine's potency, as we have previously published (Moritz et al., 2020a). Notably, the derived K_b values of 2 to 3 μM are consistent with the low (3.9–19.4 μM) plasma concentrations of ONC201 observed using dosing regimens in ongoing clinical trials (Stein et al., 2017; Prabhu et al., 2020).

Identification of D2R Residues That Are Critical for ONC201 Antagonism. To identify the receptor residues involved in ONC201 antagonism of the D2R, we performed alanine scanning mutagenesis and evaluated the functional impact of the mutations with a high throughput Ca^{2+} flux assay, as previously described (Greene et al., 2011). A library of 442 D2R constructs was first created by mutating residues 2–443 of the D2RL isoform to alanines (wild-type alanines were changed to serines) and coexpressing them in HEK293T cells with a chimeric $G\alpha_{16}$ subunit containing 44 residues of rat gustducin (Greene et al., 2011). When the wild-type D2R is expressed with the chimeric $G\alpha_{16}$ subunit containing 44 residues of rat gustducin, the addition of dopamine results in a rapid and dose-dependent Ca^{2+} flux response that can be measured using an intracellular Ca^{2+}-sensitive dye (Supplemental Fig. 1, A and B). In contrast, when the D2R is replaced with the bitter taste receptor TAS2R16, dopamine fails to induce Ca^{2+} flux indicating

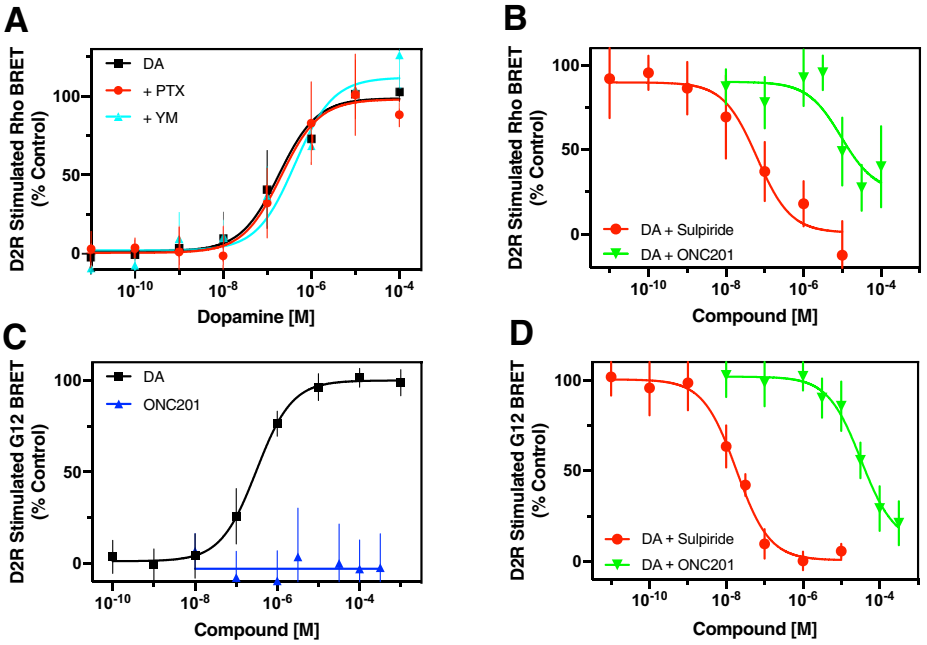

Fig. 6. Functional effects of ONC201 on D2R-mediated activation of Rho and G_{12}. HEK293 cells were transiently cotransfected with the D2R and either the Rho or G_{12} BRET biosensors, and dopamine-stimulated BRET responses were measured as described in the *Materials and Methods*. Data are expressed as a percentage of the maximum dopamine response (% control) in each assay and represent the mean ± S.D. values from 3 experiments each performed in triplicate. EC_{50} or IC_{50} values are expressed as mean values (95% CI). (A) Dopamine dose-dependently stimulated Rho activation with an EC_{50} of 185 nM [97–385]. Concurrent treatment of the cells with 200 nM YM-254890 (+YM) or overnight treatment with 100 ng/ml +PTX resulted in dopamine EC_{50} values of 430 nM [162–986] and 207 nM [99–447], respectively, which were not significantly different from control values. (B) Rho activation (BRET) was stimulated with an EC_{80} concentration of dopamine (1 μM) and treated with the indicated concentrations of sulpiride or ONC201 resulting in IC_{50} values of 63 nM [17–198] and 9.4 μM [3.3–35], respectively. (C) Dopamine dose-dependently stimulated G_{12} activation with an EC_{50} of 310 nM [216–442], whereas ONC201 had no stimulatory effect. (D) G_{12} activation (BRET) was stimulated with an EC_{80} concentration of dopamine (1 μM) and treated with the indicated concentrations of sulpiride or ONC201 resulting in IC_{50} values of 18 nM [12–27] and 33 μM [20–55], respectively.

specificity of the dopamine response for the D2R (Supplemental Fig. 1B). ONC201 was found to inhibit the dopamine-stimulated Ca^{2+} flux mediated by the wild-type D2R in a dose-dependent fashion with an IC_{50} of 21.5 μM (Supplemental Fig. 1, C and D), comparable to the ONC201 IC_{50} values observed in other D2R functional assays (*vide supra*). The entire library of 442 mutant D2R constructs was next screened for Ca^{2+} flux activity using an ~EC_{80} concentration (1 nM) of dopamine (Supplemental Fig. 1E). Dopamine-stimulated Ca^{2+} flux was observed with most of the D2R mutants, although their responses tended to be less robust than those observed with the wild-type D2R. Notably, we did not attempt to normalize these data for receptor expression levels. This alanine scan also identified 28 D2R residues that, when mutated, led to a dopamine response that was more than two S.D.s below the average Ca^{2+} response or, in some cases, completely negated (Supplemental Fig. 1E, Supplemental Table 2).

We next evaluated the ability of ONC201 to inhibit dopamine-stimulation of the mutant D2R constructs with the exclusion of the 28 constructs listed in Supplemental Table 2. Ca^{2+} flux was first measured in response to 1 nM dopamine for each of the 442 D2R mutants, with the data expressed as a percentage of the wild-type D2R response (Fig. 8, light green symbols). Secondly, we measured the dopamine-stimulated Ca^{2+} response for each of the mutants in the presence of 100 μM ONC201, a concentration that inhibits the dopamine response in the wild-type D2R by 100% (Supplemental Fig. 1, C and D). On average, across the entire library of mutant D2R constructs, 100 μM ONC201 inhibited the dopamine-stimulated Ca^{2+} response by ~75% (Fig. 8, cyan symbols). Notably, however, we identified eight mutant D2R constructs that exhibited Ca^{2+} flux responses greater than two S.D.s above the average responses observed in the presence of 100 μM ONC201 (Fig. 8, red residues, Table 2), suggesting that these residues are important for antagonism of the D2R by ONC201. These eight residues are also mapped on the D2R-risperidone crystal structure (Fig. 8B) (Wang et al., 2018). Table 2 further illustrates the impact of these mutations on ONC201's ability to antagonize the D2R-mediated Ca^{2+} response; note the complete inhibition by 100 μM ONC201 in the wild-type D2R and relative lack of inhibition in the mutant constructs.

We then investigated the effects of the eight identified mutations on dopamine signaling using different functional assays for the D2R. Figure 9A shows dopamine stimulation of D2R-mediated G_o activation using a BRET-based assay (Sanchez-Soto et al., 2020) with the average EC_{50} values for dopamine listed in Table 3. As can be seen, the mutant EC_{50} values vary within 2-fold of the wild-type EC_{50} value, while the E_{max} values are nearly identical (Fig. 9A), suggesting that the mutations have very little effect on dopamine-stimulation of the D2R. Using this same assay, we also examined the ability of the orthosteric antagonist sulpiride to inhibit dopamine-stimulated G_o activation (Fig. 9B) with the average IC_{50} values listed in Table 3. Somewhat greater variability in the IC_{50} values for sulpiride was observed with the mutant

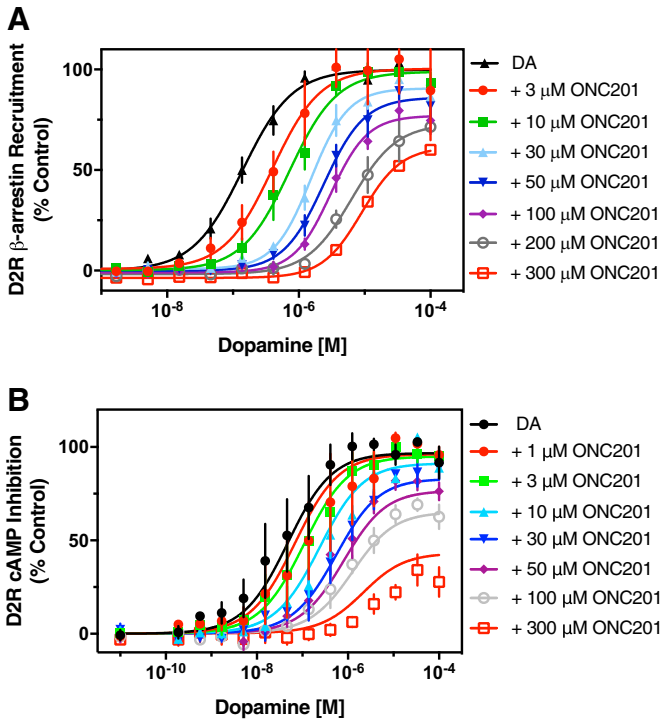

Fig. 7. Curve-shift assays indicate that ONC201 behaves in an allosteric manner with dopamine at the D2R. D2R-mediated β-arrestin recruitment assays (A) or cAMP inhibition assays (LANCE) (B) were conducted by stimulating the receptor with the indicated concentrations of dopamine with or without various concentrations of ONC201, as described in the *Materials and Methods*. For the cAMP assay, the cells were preincubated with 10 μM forskolin to stimulate cAMP production. Data are expressed as a percentage of the maximum dopamine response seen in the absence of ONC201 (% control). Data points represent the mean ± S.D. of at least three independent experiments each performed in triplicate. The curves represent the best global fit of grouped data as determined using an operational model of allosterism (Leach et al., 2007), as described in the *Materials and Methods*, with the corresponding functional parameters being summarized in Table 1.

receptors, however, these varied by less than 3-fold with the exception of the I397A mutant, where sulpiride was ~4-fold less potent compared with the wild-type D2R. These results suggest that, with the possible exception of I397A, these mutations have minimal effects on the ability of sulpiride to antagonize the D2R. To confirm these results, we used another D2R-mediated functional assay: inhibition of cAMP accumulation using a CAMYEL BRET biosensor (Sanchez-Soto et al., 2020). Figure 9 shows concentration-response curves for dopamine stimulation (Fig. 9C) or sulpiride inhibition (Fig. 9D) of the cAMP response mediated by the D2R wild-type or mutant receptors with their corresponding EC_{50} and IC_{50} values displayed in Table 3. As can be seen, other than the slight ~4-fold decrease in potency for sulpiride exhibited by the I397A construct, these mutations appear to have minimal effects on the interactions of either dopamine or sulpiride with the D2R.

We next evaluated the ability of ONC201 to inhibit dopamine stimulation of the D2 wild-type or mutant receptors using the G_o and cAMP functional assays. Figure 10A shows concentration-response curves for ONC201 inhibition of dopamine stimulation of Go BRET activation with the mean IC_{50} values displayed in Table 3. As can be seen, three of the mutations, V91A, E95A, and I397A produced a greater than 5-fold decrease in ONC201 potency for inhibiting the G_o response, whereas the other mutations were less impactful. Figure 10B shows dose-response curves for ONC201 inhibition of the dopamine-stimulated cAMP response with mean IC_{50} values displayed in Table 3. In the case of this functional response, three mutations, V91A, Y192A, and I397A, resulted in a greater than 5-fold decrease in ONC201 potency, although the IC_{50} for the E95A mutant was also increased by greater than 2-fold. In particular, the dose-response curves for V91A and I397A appear to be right-shifted by more than one log unit, although we cannot determine their IC_{50} values quantitatively. Taken together, based on the results of the Ca^{2+} flux, G_o activation, and cAMP inhibition assays, we concluded that the mutations that produced the most severe impact on ONC201's ability to antagonize the D2R were V91A, E95A, Y192A, and I397A. Note, Y192 is in close vicinity to I397 in the interface between TMs 5 and 6, while V91 and E95 are one helical turn away from each other within the extracellular portion of TM2 (*vide infra*).

Molecular Modeling Reveals Interactions of ONC201 with a D2R Allosteric Pocket. Given the identification of D2R residues that are important for ONC201 activity, we

TABLE 1
Functional parameters for ONC201 antagonism of D2R-mediated signaling
Data are the best fit of grouped data from at least 3 independent experiments, expressed as geometric means [95% confidence interval].

Assay	$Log\tau_A^a$	$Log\tau_B^b$	pK_A^c	pK_B^d	$Log\alpha^e$	$Log\beta^f$	slope^g
				K_B	α		
β-arrestin	1.57 [0.73–2.40]	−3.00	5.26 [4.39–6.14]	5.53 [5.42–5.64] (3 μM)	−0.70 [−1.59–0.20] (0.2)	−3.00	1.21 [1.06–1.35]
cAMP	1.68 [1.21–2.23]	−3.00	5.62 [5.05-6.15]	5.64 [5.37–5.92] (2.3 μM)	−0.28 [−0.85 – 0.34] (0.5)	−3.00	0.88 [0.77–1.02]

β-arrestin and cAMP experiments were performed as described in Figs. 7A and B and the data were analyzed according to an operational model of allosterism (Leach et al., 2007) as described in the *Materials and Methods* to derive estimates of:
[a]the logarithm of dopamine efficacy,
[b]the logarithm of ONC201 efficacy constrained to −3 to indicate ONC201 displays no detectable agonist efficacy,
[c]the negative logarithm of dopamine affinity,
[d]the negative logarithm of ONC201 affinity,
[e]the logarithm of the binding cooperativity between dopamine and ONC201,
[f]the logarithm of the magnitude of the allosteric effect of the modulator on the efficacy of the orthosteric agonist, constrained to −3 indicating that ONC201 exhibits a very high level of negative cooperativity,
[g]the Hill slope.

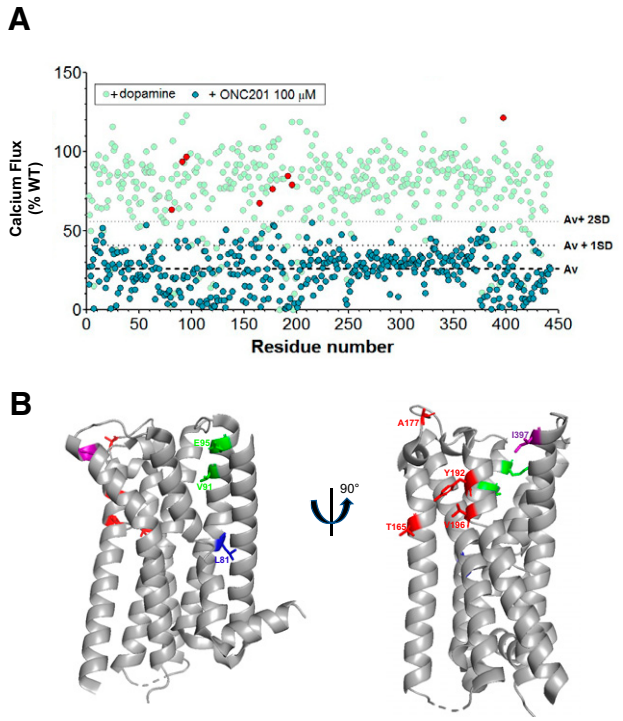

Fig. 8. Alanine scanning mutagenesis identifies amino acids important for ONC201 antagonism of D2R signaling. HEK293T cells were transiently transfected with the wild-type (WT) D2R or D2R mutants and a chimeric $G\alpha_{16}$ subunit. After 22 hours, calcium flux experiments were performed as described in the *Materials and Methods*. (A) Ca^{2+} flux was measured in response to 1 nM dopamine for each of the 442 D2R clones shown in Supplemental Fig. 1E and expressed as a percentage of the wild-type D2R response (light green symbols). For each D2R clone in the alanine-scan library, Ca^{2+} flux was also measured in response to 1 nM dopamine in the presence of 100 μM ONC201 and expressed as a percentage of the dopamine-stimulated response for the wild-type D2R (cyan and red symbols). The data represent average values from three experiments. Mutant clones (red symbols) were considered to be critical for ONC201 inhibition if they demonstrated Ca^{2+} flux values greater than 2 S.D.s above the average flux value (AV + 2 S.D.) observed in the presence of 100 μM ONC201. These eight residues (red symbols) are listed in Table 2. (B) The eight residues identified in (A) are depicted in the risperidone-D2R crystal structure [(Wang et al., 2018), PDB 6CM4]. Four colors depict the distinct geographic regions of these eight residues.

TABLE 2
D2R residues critical for ONC201 inhibition of dopamine-stimulated Ca^{2+} flux

D2R Mutation*	DA-stimulated Ca^{2+} Flux	DA-stimulated Ca^{2+} Flux + ONC201
	% WT	*% WT*
WT	100	0
L81A	83	63
V91A	119	94
E95A	123	97
T165A	92	67
A177S	85	77
Y192A	64	85
V196A	119	79
I397A	105	89

*Residues were identified from the analysis shown in Figure 8A. Calcium flux was measured in response to 1 nM dopamine (DA) with or without 100 μM ONC201 as described in Figure 8 and expressed as a percentage of the WT D2R response in the absence of ONC201.

sought to further characterize the binding pose of ONC201 at the D2R using computational modeling and simulation approaches. We first performed molecular docking of ONC201 using an inactive state structure of the D2R as represented by the crystal structure of the receptor in complex with the antagonist spiperone (Im et al., 2020), given that our radioligand binding assays were carried out with [^{3}H]methyspiperone and that the binding poses of various antagonists can affect the size and shape of the binding pocket even within inactive states (Lane et al., 2020). Our pKa prediction indicated that, unlike most aminergic receptor ligands (Michino et al., 2015), ONC201 lacks a protonatable nitrogen at physiologic pH, which is necessary to form an ionic interaction with the conserved D114$^{3.32}$ residue in TM3 [superscripts denote Ballesteros-Weinstein numbering (Ballesteros and Weinstein, 1995)]. Indeed, our docking results show that ONC201 fails to form a salt bridge with D114$^{3.32}$ (Fig. 11). Instead, ONC201 adopts a binding pose such that the unsubstituted phenyl ring (Fig. 1A) enters a secondary binding pocket (SBP) formed by the interface between TMs 2 and 7 and forms interactions with V91$^{2.61}$ and E95$^{2.65}$ (Fig. 11, A and B). Figure 11 also illustrates the binding pose of spiperone within the orthosteric binding site of the D2R as determined from the crystal structure (Im et al., 2020). The binding pose of ONC201 suggests that it protrudes into the orthosteric space occupied by spiperone in the inactive D2R structure (Fig. 11, A and B) and is consistent with the ability of ONC201 to compete with [^{3}H]methyspiperone for binding to the D2R (Fig. 2).

Using an active state structure of the D2R (Yin et al., 2020), we then docked ONC201 to the extracellular vestibule of the receptor (Yin et al., 2020) with dopamine bound to the orthosteric binding site. From preliminary docking results, we identified two representative poses; one is located near Y192$^{5.41}$ and I397$^{6.59}$ (pose 1), while the other involves interactions with V91$^{2.61}$ and E95$^{2.65}$ (pose 2). However, we could not find any ONC201 pose where it simultaneously interacts with all four of these residues, which is geometrically unlikely as Y192$^{5.41}$/I397$^{6.59}$ and V91$^{2.61}$/E95$^{2.65}$ are on the two opposite ends of the extracellular vestibule. To evaluate the stability of these two poses, we carried out molecular dynamics (MD) simulations (see *Materials and Methods*). Our results show that in pose 1, the hydrophobic and aromatic interactions formed between the toluene moiety of ONC201 and I397$^{6.59}$ and Y192$^{5.41}$ are stable to the extent of our simulations (Fig. 12A), while in pose 2, ONC201 persistently interacts with residues V91$^{2.61}$ and E95$^{2.65}$ in the SBP (Fig. 12B), as was observed in the inactive state of the D2R (Fig. 11). Notably, however, in either pose, ONC201 does not overlap with the space occupied by dopamine within the orthosteric binding site (Fig. 12B).

Discussion

As antagonism of the D2R has been suggested to contribute to ONC201's anticancer activity (Madhukar et al., 2019), we wished to characterize the pharmacological interactions of this compound with the D2R and related dopamine receptor subtypes. Our results revealed that ONC201 was highly selective for the D2R and D3R with little to no activity at related biogenic amine and other

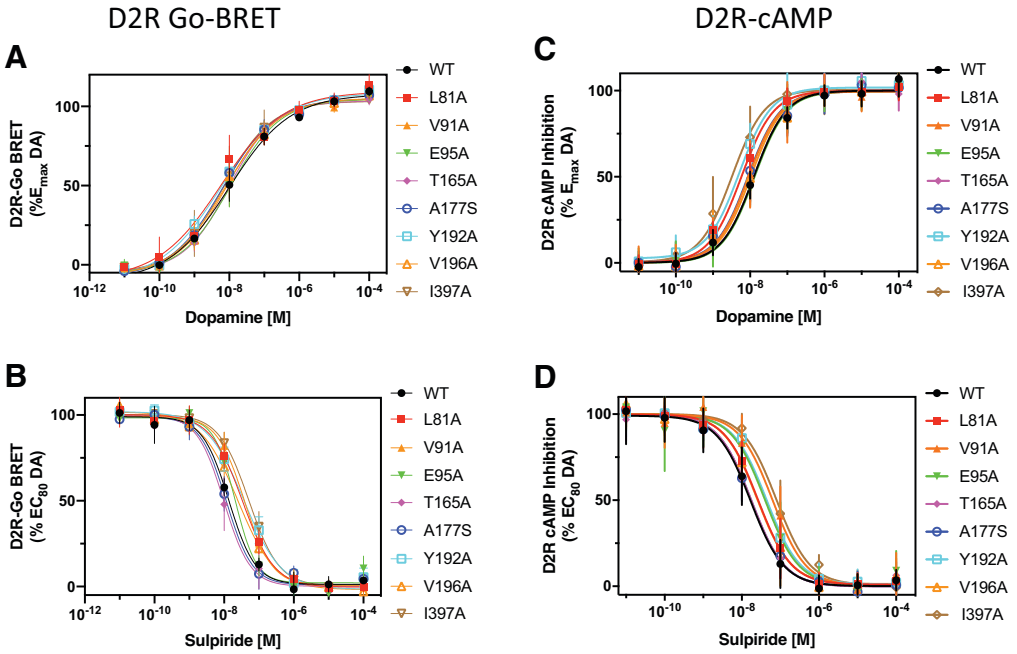

Fig. 9. D2R mutants that affect ONC201 antagonism are not impaired in dopamine stimulation or sulpiride antagonism of G protein-mediated signaling. (A) HEK293 cells were transfected with the untagged wild-type D2R, or the indicated D2R mutants, along with Gαo1-RLuc8, Gγ2-mVenus, and Gβ1. After 48 hours, dopamine-stimulation of G_o activation was assessed using a BRET assay as described in the *Materials and Methods*. The dopamine EC_{50} values for each D2R construct are shown in Table 3. (B) The cells were transfected as in (A) followed by stimulation with an EC_{80} concentration of dopamine (7 nM) and increasing concentrations of the orthosteric antagonist sulpiride. BRET ratio values were determined and the sulpiride IC_{50} values for each D2R construct are shown in Table 3. (C) HEK293 cells were transfected with the untagged wild-type D2R, or the indicated D2R mutants, along with the CAMYEL cAMP BRET biosensor. After 48 hours, the cells were incubated with 10 μM forskolin to stimulate cAMP accumulation, plus the indicated concentrations of dopamine. BRET ratio values were determined as described in the *Materials and Methods* with the dopamine EC_{50} values shown in Table 3. (D) The cells were transfected and treated as in (C) followed by stimulation with an EC_{80} concentration of dopamine (25 nM) and increasing concentrations of sulpiride. BRET ratio values were determined, and the sulpiride IC_{50} values for each D2R construct are shown in Table 3. In each panel, the data are expressed as a percentage of the wild-type D2R response. Data points represent the mean ± S.D. of at least three independent experiments each performed in triplicate.

GPCRs. Radioligand binding competition experiments using [^{3}H]methylspiperone revealed that ONC201 exhibited Ki values of 67 μM and 30 μM for the D2R and D3R, respectively, suggesting that ONC201 actually exhibits higher affinity for the D3R versus the D2R. It should be noted, however, that our derivation of these Ki values using the Cheng-Prusoff equation (Cheng and Prusoff, 1973) assumes a completely competitive interaction between ONC201 and the radioligand, which, in fact, might be more complicated in nature (*vide infra*). In contrast, when assessed using a β-arrestin recruitment functional assay, ONC201 exhibited greater potency for antagonizing the dopamine-stimulated response at the D2R (IC_{50} = 11 μM) when compared with the D3R (IC_{50} = 21 μM). The reason for the different D2R/D3R selectivity in the binding and functional assays may be related to the different potencies of dopamine for stimulating β-arrestin recruitment to the D2R (dopamine EC_{50} = 58 nM) versus the D3R (dopamine EC_{50} = 3 nM), and that the interactions of ONC201 with the receptors may differ between the assays (*vide infra).* Finally, ONC201 was found to exhibit little affinity for the D4R as assessed using both β-arrestin recruitment and cAMP functional assays.

Notably, a structurally related isomer of ONC201 that is inactive in inhibiting the proliferation of cancer cells (Wagner et al., 2014) was similarly ineffective in antagonizing the D2R consistent with the idea that reduced D2R signaling contributes to the anticancer activity of ONC201. In addition to antagonizing the D2R, ONC201 also activates mitochondrial ClpP, which inhibits cancer cell proliferation (Graves et al., 2019; Ishizawa et al., 2019), suggesting that dual D2R inhibition and ClpP activation might have additive or synergistic effects to cause cancer cell death. Notably, many Food and Drug Administration–approved antipsychotic drugs, whose mechanism of action is D2R antagonism (Kapur and Remington, 2001; Masri et al., 2008), also exhibit anticancer effects, albeit with variable efficacies and potencies typically lower than their affinities for the D2R (Lee et al., 2016; Gao et al., 2018; Roney and Park, 2018; Weissenrieder et al., 2019; Bhat et al., 2020). Patients taking antipsychotics have also been shown to exhibit a decreased incidence of cancers such as glioblastoma (Gao et al., 2018). However, to date, no antipsychotic drug has been repurposed as a cancer therapeutic, suggesting that D2R antagonism alone may be insufficient to effectively induce cancer cell death, and that modulation of additional targets (e.g., ClpP activation) may be needed to be clinically efficacious as an anticancer therapeutic. In addition, drugs that exhibit a highly negative modulatory effect on dopamine efficacy might be particularly effective in blocking D2R signaling in tumors with high local concentrations of dopamine that might overcome competitive antagonists, which comprise the vast majority of antipsychotics.

Importantly, the specific D2R-mediated signaling pathways that are associated with the therapeutic effects of

TABLE 3

Pharmacological Characterization of D2R Mutants using Go and CAMYEL BRET Assays.

EC_{50} and IC_{50} values were derived as described in Figs. 9 and 10 via nonlinear regression of individual experiments normalized to the dopamine-stimulated wild-type (WT) D2R control. For each D2R mutant, the EC_{50} or IC_{50} value was divided by the wild-type EC_{50} or IC_{50} value to derive the corresponding wild-type ratio. Data are expressed as geometric means [95% confidence interval].

		WT	L81A	V91A	E95A	T165A	A177S	Y192A	V196A	I397A
Dopamine	Go	9.9 nM	5.7 nM	7.7 nM	11 nM	10 nM	6.5 nM	5.9 nM	8.3 nM	7 nM
	EC_{50}	[6.3–15]	[1.5–14]	[4.3–13]	[6.8–17]	[7.2–14]	[4.5–9.3]	[3.8–8.8]	[5.8–12]	[3.4–13]
	WT Ratio	1	0.6	0.8	1.1	1	0.7	0.6	0.8	0.7
	cAMP EC_{50}	12 nM	5.8 nM	9 nM	13 nM	12.7 nM	8.7 nM	5.1 nM	10 nM	3.3 nM
		[10–16]	[4.8–7]	[6–13]	[9.7–17]	[9.7–17]	[6.3–12]	[3.6–7.2]	[7.5–14]	[2–4.8]
	WT Ratio	1	0.5	0.7	1	1	0.7	0.4	0.8	0.3
Sulpiride	Go	13 nM	34 nM	38 nM	21 nM	9.8 nM	12 nM	37 nM	25 nM	51 nM
	IC_{50}	[10–20]	[24–46]	[29–50]	[29–50]	[6.6–15]	[8–17]	[25–55]	[19–33]	[39–67]
	WT Ratio	1	2.6	2.9	1.6	0.8	0.9	2.9	2.1	3.9
	cAMP	17 nM	26 nM	63 nM	40 nM	18 nM	18 nM	43 nM	25 nM	78 nM
	IC_{50}	[12–25]	[20–35]	[42–92]	[24–65]	[12–26]	[13–23]	[31–61]	[17–38]	[59–104]
	WT Ratio	1	1.5	3.7	2.4	1	1	2.5	1.5	4.6
ONC201	Go	21 μM	45 μM	>100 μM	>100 μM	32 μM	31 μM	40 μM	50 μM	>100 μM
	IC_{50}	[12–40]	[29–71]			[15–67]	[17–60]	[25–66]	[30–87]	
	WT Ratio	1	2	>5	>5	1.5	1.5	1.9	2.4	>5
	cAMP	23 μM	46 μM	>100 μM	55 μM	12 μM	29 μM	>100 μM	45 μM	>100 μM
	IC_{50}	[16–33]	[20–122]		[28–126]	[9–16]	[14–63]		[23–97]	
	WT Ratio	1	2	>5	2.4	0.5	1.3	>5	2	>5

N = 3–5 experiments run in triplicate.

ONC201 are not clear. In this regard, it was of interest to observe that the D2R activated G_{12} and Rho signaling. Typically, the D2R signals through the $G_o/G_i/G_z$ family of G proteins (Beaulieu and Gainetdinov, 2011) and is predominantly coupled to G_o in the brain (Jiang et al., 2001; Masuho et al., 2021). In fact, to our knowledge, this is the first evidence that the D2R is capable of activating of G_{12}. Notably, $G\alpha_{12/13}$, $G\alpha_{12/13}$-coupled GPCRs, and their effectors, including Rho, are overexpressed in a number of different cancers [reviewed in (Arang and Gutkind, 2020)]. Further, $G\alpha_{12/13}$ have been investigated as drivers of cellular transformation, cancer progression, and metastatic potential in a variety of cell types (Arang and Gutkind, 2020). Theoretically, in a cell type endogenously expressing the D2R and G_{12} (or possibly G_{13}, although we did not examine D2R-G_{13} interactions), mutations leading to activation or upregulation of either protein could result in aberrant D2R-G_{12} coupling and downstream signaling, such as Rho activation, ultimately leading to cancer initiation. In this scenario, ONC201 might be effective in dampening tumor cell growth through inhibiting D2R-G_{12} signaling, although as noted above, engagement of other targets might also be important. It will be of interest to examine D2R-G_{12} signaling in cancer cell types (e.g., gliomas) in future experimentation.

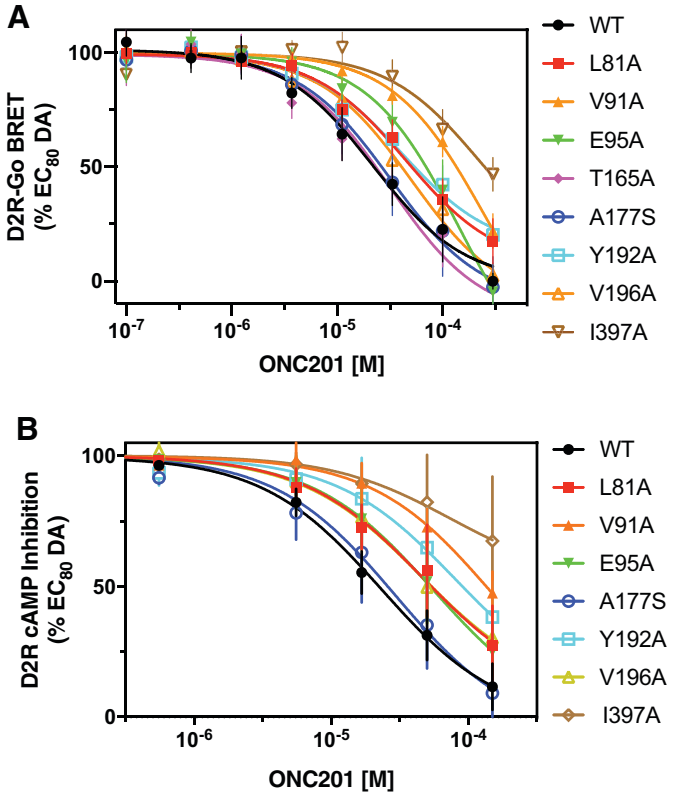

Fig. 10. ONC201 antagonism of D2R-mediated G protein-mediated signaling is severely impaired in select D2R point mutants. (A) Go BRET activation assays were performed as described in Fig. 9 and the Materials and Methods. Cells were incubated with an EC_{80} concentration of dopamine (7 nM) and increasing concentrations of ONC201. BRET ratios were determined, and the data are expressed as a percentage of the wild-type D2R response. The mean IC_{50} values for each D2R construct are shown in Table 3. (B) CAMYEL BRET cAMP inhibition assays were performed as described in Fig. 9 and the Materials and Methods. The cells were incubated with an EC_{80} concentration of dopamine (25 nM) and increasing concentrations of ONC201. BRET ratios were determined, and the data are expressed as a percentage of the maximum wild-type D2R response. The mean IC_{50} values for each D2R construct are shown in Table 3. Data points represent the mean ± S.D. of at least three independent experiments each performed in triplicate.

As noted above, the apparent affinity of ONC201 for the D2R was between 2- to 6-fold lower in the radioligand binding competition assays using [^{3}H]methylspiperone (Ki = 67 μM) when compared with antagonizing dopamine action in the functional assays: (IC_{50} values) β-arrestin recruitment (11 μM), cAMP inhibition (9.3 μM), Ca^{2+} mobilization (21.5 μM), G_{12} activation (33 μM), and Rho activation (9.4 μM). If an antagonist is competitive in nature, then its K_b value can be derived from IC_{50} values by performing functional curve-

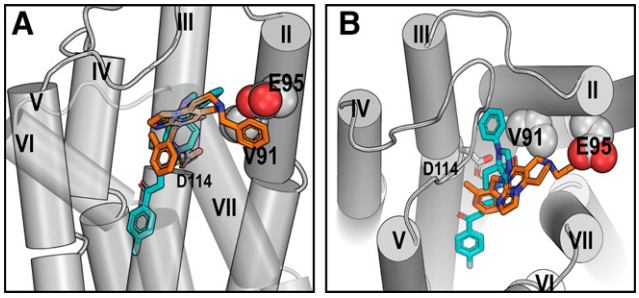

Fig. 11. The binding pose of ONC201 in the inactive state of the D2R overlaps with that of spiperone. Molecular docking was performed as described in the Methods using a model (see Supplement for PDB file) of the D2R in an inactive state based on a crystal structure of the D2R in complex with the antagonist spiperone (Im et al., 2020) (PDB: 7DFP). The superposition of the spiperone (colored in cyan) and ONC201 (colored in orange) poses are shown both from a side view (A) and an extracellular view (B) of the receptor's TM regions. Receptor residues within the orthosteric pocket (D114) and allosteric pocket (V91 and E95) are designated.

shift experiments and Schild plot analyses. However, it was clear from the functional curve-shift data shown in Fig. 7 that ONC201 exhibited mixed antagonism of dopamine signaling through the D2R. We thus analyzed the ONC201 curve-shift data using an operational model of allostery (Leach et al., 2007) to derive K_b values for antagonism of dopamine-stimulated β-arrestin recruitment (K_b = 3 μM) and inhibition of cAMP accumulation (K_b = 2.3 μM). Thus, the functional potency of ONC201 for antagonizing dopamine-stimulation of the D2R actually appears to be ~2 to 3 μM. Interestingly, these analyses also revealed that ONC201 displays little apparent cooperativity with dopamine affinity but mostly exhibits a negative modulatory effect on dopamine efficacy, suggestive of an allosteric mechanism of action.

To further understand the mechanism of action of ONC201 at the D2R, we identified the receptor residues important for ONC201 to antagonize dopamine signaling. This initially involved alanine scanning mutagenesis while evaluating the functional activity of the receptor using a high throughput Ca^{2+} mobilization assay. This endeavor identified eight receptor residues that, when mutated to alanines, significantly decreased the ability of a single high concentration (100 μM) of ONC201 to inhibit dopamine-stimulated Ca^{2+} mobilization

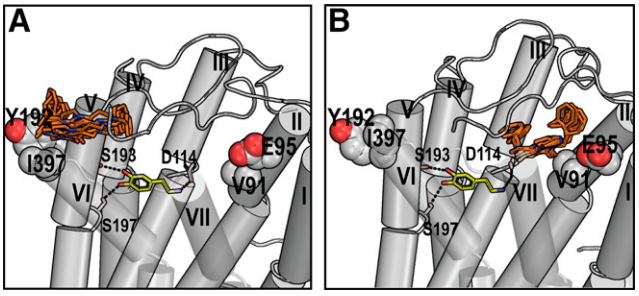

Fig. 12. The two possible ONC201 binding poses in the extracellular vestibule of the D2R in the active state. Molecular docking was performed as described in the Methods using an active state structure of the D2R (Yin et al., 2020) (PDP: 6VMS). Poses 1 (A) and 2 (B) of ONC201 (colored in orange) in the extracellular vestibule are shown with dopamine (colored in yellow) bound to the orthosteric binding site (see Supplement for PDB files of poses 1 and 2). Orthosteric residues D114, S193, and S197 form direct interactions with dopamine. For each pose, MD frames were extracted every 60 ns for the last 300 ns of their corresponding MD trajectories.

mediated by the mutant receptors. More comprehensive analyses of the D2R mutants by collecting full ONC201 dose-response curves using G_o activation and cAMP inhibition assays showed that mutations of four specific residues, $V91^{2.61}$, $E95^{2.65}$, $Y192^{5.41}$, and $I397^{6.59}$, produced the most severe impact on ONC201's ability to antagonize dopamine-stimulated signaling. Notably, two of these residues, $V91^{2.61}$ and $E95^{2.65}$, reside within a SBP formed by the interface between TMs 2 and 7 and have been shown to be involved in allosteric modulation of the D2R by bitopic and negative allosteric modulators (NAMs) (Draper-Joyce et al., 2018; Verma et al., 2018; Klein Herenbrink et al., 2019).

Using the mutational data as a guide, we sought to characterize the binding pose of ONC201 with the D2R using computational modeling and simulation studies. Initial molecular docking of ONC201 using the crystal structure of an inactive state of the receptor bound to spiperone (Im et al., 2020) suggested that a pendant phenyl ring can enter the SBP described above and form hydrophobic and polar interactions with $V91^{2.61}$ and $E95^{2.65}$, respectively. Notably, this binding pose also suggests that the imipridone core of ONC201 protrudes into the orthosteric space occupied by spiperone, which likely explains its ability to inhibit [^{3}H]methylspiperone binding, albeit with low affinity. These results suggest that ONC201 can interact with the D2R in a bitopic manner, where the imipridone core of the molecule overlaps with the orthosteric binding site while a phenyl ring engages a secondary allosteric binding pocket.

In contrast, when we docked ONC201 at an active state D2R structure (Yin et al., 2020) with dopamine occupying the orthosteric site, we could not identify a pose where ONC201 simultaneously interacts with all four residues ($V91^{2.61}$, $E95^{2.65}$, $Y192^{5.41}$, and $I397^{6.59}$) that were shown to be extremely important for antagonism of the receptor. However, two poses were stable after microsecond scale MD simulations; one involves ONC201 interactions with $Y192^{5.41}$ and $I397^{6.59}$ (pose 1), whereas in the other pose ONC201 interacts with $V91^{2.61}$ and $E95^{2.65}$ (pose 2). To integrate the experimental observations, we propose that residues $Y192^{5.41}$ and $I397^{6.59}$ interact with ONC201 near an entry point to the extracellular vestibule at the extracellular interface of TM5 and TM6 followed by a transition of ONC201 to a pose near the interface between TM2 and TM7 where it interacts with $V91^{2.61}$ and $E95^{2.65}$ within the SBP. Notably, in either pose, ONC201 does not overlap with the space occupied by dopamine within the orthosteric binding site, suggesting that it acts as a NAM to inhibit dopamine-stimulated receptor signaling. These results are in good agreement with the curve-shift experiments (*vide supra*), suggesting that ONC201 has little effect on dopamine's affinity but exhibits strong negative cooperativity with dopamine's efficacy.

In summary, ONC201 is a novel antagonist of the D2R with demonstrated efficacy in the treatment of various cancers, especially high-grade glioma. It demonstrates a novel bitopic/NAM mechanism of action that may explain its high selectivity for the D2R and some of its clinical anticancer properties that are distinct from other D2R antagonists widely used for the treatment of schizophrenia and other neuropsychiatric disorders.

Authorship Contributions

Participated in research design: Free, Xie, Namkung, Prabhu, Sibley, Laporte, Shi, Allen.

Conducted experiments: Cuoco, Xie, Namkung, Willette, Day.

Contributed new reagents or analytic tools: Namkung, Laporte.

Performed data analysis: Free, Cuoco, Xie, Namkung, Willette, Day, Sanchez-Soto, Lane, Shi.

Wrote or contributed to the writing of the manuscript: Free, Namkung, Lane, Laporte, Shi, Allen, Sibley.

References

Allen JE, Crowder RN, and El-Deiry WS (2015) First-in-class small molecule ONC201 induces DR5 and cell death in tumor but not normal cells to provide a wide therapeutic index as an anti-cancer agent. *PLoS One* **10**:e0143082.

Allen JE, Krigsfeld G, Mayes PA, Patel L, Dicker DT, Patel AS, Dolloff NG, Messaris E, Scata KA, Wang W, et al. (2013) Dual inactivation of Akt and ERK by TIC10 signals Foxo3a nuclear translocation, TRAIL gene induction, and potent antitumor effects. *Sci Transl Med* **5**:171ra17.

Arang N and Gutkind JS (2020) G protein-coupled receptors and heterotrimeric G proteins as cancer drivers. *FEBS Lett* **594**:4201–4232.

Ballesteros JA and Weinstein H (1995) Integrated methods for the construction of three-dimensional models and computational probing of structure-function relations in G protein-coupled receptors. *Methods in Neuroscience* **25**:366–428.

Beaulieu JM and Gainetdinov RR (2011) The physiology, signaling, and pharmacology of dopamine receptors. *Pharmacol Rev* **63**:182–217.

Bhat K, Saki M, Vlashi E, Cheng F, Duhachek-Muggy S, Alli C, Yu G, Medina P, He L, Damoiseaux R, et al. (2020) The dopamine receptor antagonist trifluoperazine prevents phenotype conversion and improves survival in mouse models of glioblastoma. *Proc Natl Acad Sci USA* **117**:11085–11096.

Bowers K, Chow E, Xu H, Dror R, Eastwood M, Gregersen B, Klepeis J, Kolossvary I, Moraes M, Sacerdoti F, et al.(2006) Proceedings of the 2006 ACM/IEEE conference on Supercomputing, Association for Computing Machinery, Tampa, Florida.

Caragher SP, Shireman JM, Huang M, Miska J, Atashi F, Baisiwala S, Hong Park C, Saathoff MR, Warnke L, Xiao T, et al. (2019) Activation of dopamine receptor 2 prompts transcriptomic and metabolic plasticity in glioblastoma. *J Neurosci* **39**:1982–1993.

Cheng Y and Prusoff WH (1973) Relationship between the inhibition constant (K1) and the concentration of inhibitor which causes 50 per cent inhibition (I50) of an enzymatic reaction. *Biochem Pharmacol* **22**:3099–3108.

Cherubini E, Di Napoli A, Noto A, Osman GA, Esposito MC, Mariotta S, Sellitri R, Ruco L, Cardillo G, Ciliberto G, et al. (2016) Genetic and functional analysis of polymorphisms in the human dopamine receptor and transporter genes in small cell lung cancer. *J Cell Physiol* **231**:345–356.

Coufal M, Invernizzi P, Gaudio E, Bernuzzi F, Frampton GA, Onori P, Franchitto A, Carpino G, Ramirez JC, Alvaro D, et al. (2010) Increased local dopamine secretion has growth-promoting effects in cholangiocarcinoma. *Int J Cancer* **126**:2112–2122.

Draper-Joyce CJ, Michino M, Verma RK, Klein Herenbrink C, Shonberg J, Kopinathan A, Scammells PJ, Capuano B, Thal DM, Javitch JA, et al. (2018) The structural determinants of the bitopic binding mode of a negative allosteric modulator of the dopamine D_2 receptor. *Biochem Pharmacol* **148**:315–328.

Fortin Ensign SP, Mathews IT, Symons MH, Berens ME, and Tran NL (2013) Implications of Rho GTPase signaling in glioma cell invasion and tumor progression. *Front Oncol* **3**:241.

Gao X, Mi Y, Guo N, Xu H, Jiang P, Zhang R, Xu L, and Gou X (2018) Glioma in schizophrenia: is the risk higher or lower? *Front Cell Neurosci* **12**:289.

Graves PR, Aponte-Collazo LJ, Fennell EMJ, Graves AC, Hale AE, Dicheva N, Herring LE, Gilbert TSK, East MP, McDonald IM, et al. (2019) Mitochondrial protease ClpP is a target for the anticancer compounds ONC201 and related analogues. *ACS Chem Biol* **14**:1020–1029.

Greene TA, Alarcon S, Thomas A, Berdougo E, Doranz BJ, Breslin PA, and Rucker JB (2011) Probenecid inhibits the human bitter taste receptor TAS2R16 and suppresses bitter perception of salicin. *PLoS One* **6**:e20123.

Harris SS and Urs NM (2021) Targeting β-arrestins in the treatment of psychiatric and neurological disorders. *CNS Drugs* **35**:253–264.

Im D, Inoue A, Fujiwara T, Nakane T, Yamanaka Y, Uemura T, Mori C, Shiimura Y, Kimura KT, Asada H, et al. (2020) Structure of the dopamine D_2 receptor in complex with the antipsychotic drug spiperone. *Nat Commun* **11**:6442.

Ishizawa J, Zarabi SF, Davis RE, Halgas O, Nii T, Jitkova Y, Zhao R, St-Germain J, Heese LE, Egan G, et al. (2019) Mitochondrial ClpP-mediated proteolysis induces selective cancer cell lethality. *Cancer Cell* **35**:721–737.e9.

Jiang LI, Collins J, Davis R, Lin KM, DeCamp D, Roach T, Hsueh R, Rebres RA, Ross EM, Taussig R, et al. (2007) Use of a cAMP BRET sensor to characterize a novel regulation of cAMP by the sphingosine 1-phosphate/G13 pathway. *J Biol Chem* **282**:10576–10584.

Jiang M, Spicher K, Boulay G, Wang Y, and Birnbaumer L (2001) Most central nervous system D2 dopamine receptors are coupled to their effectors by Go. *Proc Natl Acad Sci USA* **98**:3577–3582.

Kapur S and Remington G (2001) Dopamine D(2) receptors and their role in atypical antipsychotic action: still necessary and may even be sufficient. *Biol Psychiatry* **50**:873–883.

Klein Herenbrink C, Verma R, Lim HD, Kopinathan A, Keen A, Shonberg J, Draper-Joyce CJ, Scammells PJ, Christopoulos A, Javitch JA, et al. (2019) Molecular determinants of the intrinsic efficacy of the antipsychotic aripiprazole. *ACS Chem Biol* **14**:1780–1792.

Lane JR, Abramyan AM, Adhikari P, Keen AC, Lee KH, Sanchez J, Verma RK, Lim HD, Yano H, Javitch JA, et al. (2020) Distinct inactive conformations of the dopamine D2 and D3 receptors correspond to different extents of inverse agonism. *eLife* **9**:9.

Leach K, Sexton PM, and Christopoulos A (2007) Allosteric GPCR modulators: taking advantage of permissive receptor pharmacology. *Trends Pharmacol Sci* **28**:382–389.

Lee JK, Nam DH, and Lee J (2016) Repurposing antipsychotics as glioblastoma therapeutics: Potentials and challenges. *Oncol Lett* **11**:1281–1286.

Li J, Zhu S, Kozono D, Ng K, Futalan D, Shen Y, Akers JC, Steed T, Kushwaha D, Schlabach M, et al. (2014) Genome-wide shRNA screen revealed integrated mitogenic signaling between dopamine receptor D2 (DRD2) and epidermal growth factor receptor (EGFR) in glioblastoma. *Oncotarget* **5**:882–893.

Luderman KD, Conroy JL, Free RB, Southall N, Ferrer M, Sanchez-Soto M, Moritz AE, Willette BKA, Fyfe TJ, Jain P, et al. (2018) Identification of positive allosteric modulators of the D_1 dopamine receptor that act at diverse binding sites. *Mol Pharmacol* **94**:1197–1209.

Madhukar NS, Khade PK, Huang L, Gayvert K, Galletti G, Stogniew M, Allen JE, Giannakakou P, and Elemento O (2019) A Bayesian machine learning approach for drug target identification using diverse data types. *Nat Commun* **10**:5221.

Masri B, Salahpour A, Didriksen M, Ghisi V, Beaulieu JM, Gainetdinov RR, and Caron MG (2008) Antagonism of dopamine D2 receptor/beta-arrestin 2 interaction is a common property of clinically effective antipsychotics. *Proc Natl Acad Sci USA* **105**:13656–13661.

Masuho I, Skamangas NK, Muntean BS, and Martemyanov KA (2021) Diversity of the Gβγ complexes defines spatial and temporal bias of GPCR signaling. *Cell Syst* **12**:324–337.e5.

Meredith EJ, Holder MJ, Rosén A, Lee AD, Dyer MJ, Barnes NM, and Gordon J (2006) Dopamine targets cycling B cells independent of receptors/transporter for oxidative attack: Implications for non-Hodgkin's lymphoma. *Proc Natl Acad Sci USA* **103**:13485–13490.

Michino M, Beuming T, Donthamsetti P, Newman AH, Javitch JA, and Shi L (2015) What can crystal structures of aminergic receptors tell us about designing subtype-selective ligands? *Pharmacol Rev* **67**:198–213.

Moritz AE, Bonifazi A, Guerrero AM, Kumar V, Free RB, Lane JR, Verma RK, Shi L, Newman AH, and Sibley DR (2020a) Evidence for a stereoselective mechanism for bitopic activity by extended-length antagonists of the D_3 dopamine receptor. *ACS Chem Neurosci* **11**:3309–3320.

Moritz AE, Free RB, and Sibley DR (2018) Advances and challenges in the search for D_2 and D_3 dopamine receptor-selective compounds. *Cell Signal* **41**:75–81.

Moritz AE, Free RB, Weiner WS, Akano EO, Gandhi D, Abramyan A, Keck TM, Ferrer M, Hu X, Southall N, et al. (2020b) Discovery, optimization, and characterization of ML417: a novel and highly selective D_3 dopamine receptor agonist. *J Med Chem* **63**:5526–5567.

Mu J, Huang W, Tan Z, Li M, Zhang L, Ding Q, Wu X, Lu J, Liu Y, Dong Q, et al. (2017) Dopamine receptor D2 is correlated with gastric cancer prognosis. *Oncol Lett* **13**:1223–1227.

Namkung Y, LeGouill C, Kumar S, Cao Y, Teixeira LB, Lukasheva V, Giubilaro J, Simões SC, Longpré JM, Devost D, et al. (2018) Functional selectivity profiling of the angiotensin II type 1 receptor using pathway-wide BRET signaling sensors. *Sci Signal* **11**:eaat1631.

Prabhu VV, Madhukar NS, Gilvary C, Kline CLB, Oster S, El-Deiry WS, Elemento O, Doherty F, VanEngelenburg A, Durrant J, et al. (2019) Dopamine receptor D5 is a modulator of tumor response to dopamine receptor D2 antagonism. *Clin Cancer Res* **25**:2305–2313.

Prabhu VV, Morrow S, Rahman Kawakibi A, Zhou L, Ralff M, Ray J, Jhaveri A, Ferrarini I, Lee Y, Parker C, et al. (2020) ONC201 and imipridones: anti-cancer compounds with clinical efficacy. *Neoplasia* **22**:725–744.

Prabhu VV, Talekar MK, Lulla AR, Kline CLB, Zhou L, Hall J, Van den Heuvel APJ, Dicker DT, Babar J, Grupp SA, et al. (2018) Single agent and synergistic combinatorial efficacy of first-in-class small molecule imipridone ONC201 in hematological malignancies. *Cell Cycle* **17**:468–478.

Roney MSI and Park SK (2018) Antipsychotic dopamine receptor antagonists, cancer, and cancer stem cells. *Arch Pharm Res* **41**:384–408.

Roos K, Wu C, Damm W, Reboul M, Stevenson JM, Lu C, Dahlgren MK, Mondal S, Chen W, Wang L, et al. (2019) OPLS3e: extending force field coverage for drug-like small molecules. *J Chem Theory Comput* **15**:1863–1874.

Sachlos E, Risueño RM, Laronde S, Shapovalova Z, Lee JH, Russell J, Malig M, McNicol JD, Fiebig-Comyn A, Graham M, et al. (2012) Identification of drugs including a dopamine receptor antagonist that selectively target cancer stem cells. *Cell* **149**:1284–1297.

Sali A and Blundell TL (1993) Comparative protein modelling by satisfaction of spatial restraints. *J Mol Biol* **234**:779–815.

Sanchez-Soto M, Verma RK, Willette BKA, Gonye EC, Moore AM, Moritz AE, Boateng CA, Yano H, Free RB, Shi L, et al. (2020) A structural basis for how ligand binding site changes can allosterically regulate GPCR signaling and engender functional selectivity. *Sci Signal* **13**:eaaw5885.

Sibley DR and Monsma Jr FJ (1992) Molecular biology of dopamine receptors. *Trends Pharmacol Sci* **13**:61–69.

Stein MN, Bertino JR, Kaufman HL, Mayer T, Moss R, Silk A, Chan N, Malhotra J, Rodriguez L, Aisner J, et al. (2017) First-in-human clinical trial of oral ONC201 in patients with refractory solid tumors. *Clin Cancer Res* **23**:4163–4169.

Tegowski M, Fan C, and Baldwin AS (2019) Selective effects of thioridazine on self-renewal of basal-like breast cancer cells. *Sci Rep* **9**:18695.

Urs NM, Daigle TL, and Caron MG (2011) A dopamine D1 receptor-dependent β-arrestin signaling complex potentially regulates morphine-induced psychomotor activation but not reward in mice. *Neuropsychopharmacology* **36**:551–558.

Verma RK, Abramyan AM, Michino M, Free RB, Sibley DR, Javitch JA, Lane JR, and Shi L (2018) The E2.65A mutation disrupts dynamic binding poses of SB269652 at the dopamine D2 and D3 receptors. *PLOS Comput Biol* **14**:e1005948.

Wagner J, Kline CL, Pottorf RS, Nallaganchu BR, Olson GL, Dicker DT, Allen JE, and El-Deiry WS (2014) The angular structure of ONC201, a TRAIL pathway-inducing compound, determines its potent anti-cancer activity. *Oncotarget* **5**:12728–12737.

Wang S, Che T, Levit A, Shoichet BK, Wacker D, and Roth BL (2018) Structure of the D2 dopamine receptor bound to the atypical antipsychotic drug risperidone. *Nature* **555**:269–273.
Weissenrieder JS, Neighbors JD, Mailman RB, and Hohl RJ (2019) Cancer and the dopamine D_2 receptor: a pharmacological perspective. *J Pharmacol Exp Ther* **370**:111–126.
Yin J, Chen KM, Clark MJ, Hijazi M, Kumari P, Bai XC, Sunahara RK, Barth P, and Rosenbaum DM (2020) Structure of a D2 dopamine receptor-G-protein complex in a lipid membrane. *Nature* **584**:125–129.
Yu OM, Benitez JA, Plouffe SW, Ryback D, Klein A, Smith J, Greenbaum J, Delatte B, Rao A, Guan KL, et al. (2018) YAP and MRTF-A, transcriptional co-activators of RhoA-mediated gene expression, are critical for glioblastoma tumorigenicity. *Oncogene* **37**:5492–5507.
Yu OM and Brown JH (2015) G protein-coupled receptor and RhoA-stimulated transcriptional responses: links to inflammation, differentiation, and cell proliferation. *Mol Pharmacol* **88**:171–180.

Address correspondence to: David R. Sibley (sibleyd@ninds.nih.gov); or Joshua E. Allen (jallen@chimerix.com)